

Global detection of glacier surges from surface velocities, elevation change, and SAR backscatter data between 2000 and 2024 : a test of surge mechanism theories

Gregoire GUILLET ¹²³, Doug BENN ⁴, Owen KING ⁵, David SHEAN ¹, Erik Schytt MANNERFELT ², Romain HUGONNET ¹

¹*Department of Civil and Environmental Engineering, University of Washington, Seattle, WA, USA*

²*Department of Geosciences, University of Oslo, Oslo, Norway*

³*Geophysical Institute, University of Alaska Fairbanks, Fairbanks, AK, USA*

⁴*School of Geography and Sustainable Development, University of St-Andrews, St Andrews, UK*

⁵*School of Geography, Politics and Sociology, Newcastle University, Newcastle-Upon-Tyne, UK*

Correspondence: Gregoire Guillet <gregguillet@gmail.com>

ABSTRACT. The systematic investigation of individual glacier surges across a large statistical sample is key to a better understanding of surge mechanisms. This study introduces a consistent framework for identifying glacier surges from diverse remotely sensed datasets: NASA ITS_LIVE velocity fields, glacier thickness changes digital elevation models, and surface roughness from SAR backscatter. We combined these diverse datasets using Gaussian process modelling and signal processing approaches to generate the first worldwide inventory of glaciers with active surges between 2000 and 2024, identifying 261 surge events on 246 glaciers. We performed validation against reference data and conducted a quantitative analysis of key surge metrics - surge duration and peak surface velocity. Our results confirm 12 surge-type glaciers in the Randolph Glacier Inventory (v7). We further evaluated climatological influences on the distribution of surge-type glaciers and assessed the predictive capabilities of existing theories for surges, including hydrological and thermal controls as well as the enthalpy balance theory. In addition, we present the first global analysis of velocity time series from individual surge events, and

This is an Open Access article, distributed under the terms of the Creative Commons Attribution licence (<http://creativecommons.org/licenses/by/4.0>), which permits unrestricted re-use, distribution and reproduction, provided the original article is properly cited.

discuss terminus-type dependent dynamics. Our findings strongly support the unified enthalpy balance theory in explaining the breadth of observed surge behaviours. Finally, we report new surge onsets in glaciers quiescent since the 19th century.

1 Introduction

Glacier surges are quasi-periodic oscillations of ice flow behaviour affecting polythermal or temperate glaciers. During a surge event, a glacier flows at rates significantly higher than its baseline velocity (Jiskoot, 2011; Benn and Evans, 2014). The increase in flow velocity leads to the transfer of a substantial amount of mass from a reservoir zone to the receiving zone down the glacier (Meier and Post, 1969), which may result in a marked advance of the glacier terminus (Sund and others, 2014; Truffer and others, 2021). Surges last for a few months to years and are generally decoupled from climate trends, since many glaciers continue to surge in the current context of global glacier recession (Guillet and others, 2022; Kääb and others, 2023; Lovell and Fleming, 2023; Lovell and others, 2023), thus complicating the investigation of the glacier response to climate variability (Yde and Paasche, 2010; Benn, 2021). In this regard, the recent work of Hugonnet and others (2021) and Guillet and Bolch (2023) highlighted the need for a more comprehensive inventory of glaciers with known surge-type behaviour, as well as better constraints on the timing of surges when processing and analysing digital elevation model (DEM) time series. Surges represent transient behaviour that cannot be captured by standard space-time statistical models used to compute worldwide glacier mass loss, and thus hinder the interpretation of glacier/climate relationships. In addition, cyclical and climate-independent advances of surge-type glaciers have been documented as a significant source of repeated and widespread glacier hazards, such as glacier lake outburst floods (Round and others, 2017; Muhammad and others, 2021; Bazai and others, 2022) and complete glacier collapses (Gilbert and others, 2018; Kääb and others, 2018). The hazards associated with surge-type glaciers have far-reaching impacts, with direct implications for the local environment (Humphrey and others, 1986; Humphrey and Raymond, 1994; Merrand and Hallet, 1996; Lei and others, 2021), as well as communities downstream (Heinrichs and others, 1995; Ding and others, 2018; Gao and others, 2021; Truffer and others, 2021).

A broad variety of mechanisms have been proposed to better understand and capture surging behaviour. Seminal works by Clarke (1976) and subsequent studies (Fowler, 1987; Murray and Porter, 2001) relate

surging behaviour to transitions from frozen to temperate basal conditions while Kamb and others (1985); Kamb and Engelhardt (1987) presented surges as resulting from rapid changes in the subglacial drainage system. Other hydrological mechanisms, such as pulsed englacial water storage were described by Fatland and Lingle (2002) and further examined by Lingle and Fatland (2003). In addition, hydro-mechanical feedbacks such as interactions between till deformation and drainage efficiency (Clarke and others, 1984) or propagating waves of till failure (Nolan, 2003) have been described at various glaciers in Alaska.

A binary classification of Svalbard-type and Alaska-type surges has gained significant traction in the literature (e.g. Murray and others, 2003; Cuffey and Paterson, 2010; Paul and others, 2017; Bhambri and others, 2017; Solgaard and others, 2020; Guan and others, 2022). According to this classification, surges are driven by two distinct mechanisms at opposite ends of the glacier thermodynamic behaviour spectrum: a switch in thermal properties of the glacier bed, versus a switch in bed hydrology. The thermal switch hypothesis suggests that surges are triggered by a rapid transition from cold to warm conditions at the bed of the glacier (Fowler and others, 2001), a process limited to the surge of polythermal glaciers. During the quiescent phase, a surge-type glacier may be in a cold-based state, characterised by low basal water pressure and slow ice movement. However, as external factors such as increased meltwater input or changes in thermal gradients warm the glacier bed, the glacier may transition to a temperate-based state. This transition leads to enhanced basal sliding, reduced friction, and increased ice flow, which triggers a surge. The surge ends when the glacier reverts to a cold-based state due to decreased meltwater input or cooling of the glacier bed. The hydrological switch hypothesis states that quiescence results from a distributed subglacial drainage system that efficiently evacuates meltwater. If the drainage system becomes inefficient, water accumulates at the glacier-bed interface, leading to an increase in subglacial water pressure, which results in acceleration of glacier flow, effectively triggering the surge. The surge ends when the drainage system switches back to a more efficient state (Kamb and others, 1985).

More recently, Sevestre and Benn (2015), Benn and others (2019a) and Benn and others (2023) proposed a unifying hypothesis based on the enthalpy balance theory. The enthalpy balance framework formulates surging as an imbalance between potential energy, thermal energy, and basal water content as a trigger for primary flow acceleration. As flow accelerates, frictional heating at the base of the glacier leads to enhanced meltwater production, supported by the influx of additional meltwater through surface-to-bed drainage, resulting in a positive sliding/heating feedback. The surge ends once the subglacial drainage system has evacuated the surplus enthalpy from the bed (Benn and others, 2019a). The enthalpy balance

hypothesis was supported by the global statistical analysis of glacier surges conducted by Sevestre and Benn (2015), although the underlying data set was prepared through the compilation of surging observations in publications spanning the period 1861 to 2013 and relied on inconsistent qualitative criteria and variable methodologies. In contrast, the Svalbard vs. Alaska-type classification, including its predictions of a bimodal distribution in both peak velocity and surge duration, with differences between modes on an order of magnitude, has yet to be tested against a comprehensive global dataset. It is therefore necessary to compare both hypotheses with observational evidence obtained from a consistent quantitative methodology applied to a statistically significant number of surge events.

Lately, surge-type glaciers have received increasing attention, leading to the creation of various new global and regional inventories (Sevestre and Benn, 2015; Guillet and others, 2022; Guo and others, 2023; Lovell and others, 2023; Kääb and others, 2023). These efforts have provided a more accurate understanding of the prevalence of dynamic glacier instability on regional and global scales. However, different inventories were compiled using inconsistent diagnostic criteria and identification methods and a majority focused on the sole classification of glaciers as surge-type or non-surge-type, rather than identification and characterisation of individual surge events (e.g. as in Herreid and Truffer (2016) and Guillet and others (2022)). In addition, a common limitation of recent studies proposing surge-type glacier inventories has been the reliance on manual identification of surges from datasets with coarse temporal resolution, preventing the precise investigation of individual surge events. These limitations emphasise the clear need for a systematic and global inventory of individual surge events, derived from a consistent methodology.

This paper has two primary objectives. The first objective is to enhance existing methods for identifying glacier surges by introducing a comprehensive, consistent, and semi-automated framework for glacier surge detection that takes advantage of a variety of widely accessible remotely-sensed datasets, including glacier surface velocity, radar backscatter, and surface elevation time series. Motivated by the desire to create a transparent and explicit approach, we employ statistical modelling of glacier surface velocity, surface elevation and synthetic aperture radar (SAR) time series to compile the first consistent global inventory of surge events, providing detailed insights into the dynamic behaviour of individual tributaries within larger glacier complexes for the period between 2000 and 2024. The second objective is to leverage the systematic inventory of surge events to evaluate existing hypotheses for surge dynamics. Specifically, we test the predictive capabilities of the enthalpy balance theory in relation to the existence of an optimal climate envelope for surge-type glaciers, as well as its unifying character with respect to the Svalbard vs. Alaska-

type classification. We first investigate the role of climate as a fundamental control on the propensity for surging, resulting from climatic influences on mass and enthalpy budget components, before testing for the predicted existence of a continuum in peak velocity and surge duration. We further test the prediction of the Svalbard vs. Alaska-type classification, stipulating the existence of a bimodal distribution for both peak velocity and surge durations, with an identifiable order-of-magnitude difference between modes.

Beyond the identification of glaciers that experienced surges since the beginning of the 21st century, this work aims to prepare the first homogeneous catalogue of surge events. Here we incorporate crucial quantitative information about each event, and provide an important step toward a standardised community approach to studying glacier surges, similar to what has been done for earthquakes and volcanic eruptions in the past. We finally stress that the current surge event catalogue need not be static and that future or unreported surge events should be recorded and incorporated into this database.

2 Terminology and criteria for surge identification

Automating the detection of surge events requires defining a limit between what is deemed unstable (surge-type) behaviour, and what is regarded as baseline (stable) glacier behaviour. However, because of the wide spectrum of observed surge-type behaviour, surge events are often described and defined using variable terminology, and thus deriving a clear threshold between what can be considered surge-type and stable glacier behaviour is not straightforward. As a basis for defining clear thresholds between surging and stable behaviour, we first start by reviewing existing qualitative and quantitative definitions of what is considered to be surge-type behaviour and then discuss the criteria we used to automatically identify surges from the available data.

Benn and Evans (2014, pp. 186–187) describe glacier surges as "cyclic phenomena that are not directly triggered by external events, but instead result from internally driven oscillations in conditions at the bed of the glacier." Benn and Evans (2014, pp. 186–187) further mention that "maximum velocities during the active phase are typically one or two orders of magnitude higher than the velocity during the quiescent phase." In the Glossary of Glacier Mass Balance and Related Terms, Cogley and others (2010, p. 89) define a surge as "the abnormally fast flow of a glacier over a few months to years, during which the glacier margin may advance," before further emphasising that "velocities during the surge are often greater by an order of magnitude than those during the quiescent phase." Jiskoot (2011, p. 415) describes surges as quasi-periodic oscillations between long periods (tens to hundreds of years) of slow glacier flow and

shorter periods of abrupt velocity increase in velocity (typically 10 to 1000 times faster than baseline) maintained over some time (115 years); Jiskoot (2011, p. 415) further adds that during a surge, "a large volume of ice is transported from the reservoir zone (upper part) to the receiving zone (lower part) of the glacier, sometimes resulting in a marked frontal advance." Similarly, the National Snow and Ice Data Center (NSIDC) Cryosphere Glossary defines a surge as "a dramatic increase in flow rate, 10 to 100 times faster than [a glacier's] normal rate; usually surge events last less than one year and occur periodically between 15 and 100 years."

Based on these definitions, we attempt to define objective and tractable criteria for evidence of active glacier surging:

Abrupt and sustained increase in glacier surface velocity Abrupt and large increases in glacier flow velocity, sustained for at least several months, are assumed to indicate surging (see Section 3.2.2 for more information), which we typically identify here as accelerations in the flow regime of a glacier. Although many existing definitions involve a surface velocity of at least ten times that observed during the quiescent phase, here we follow the reasoning of Guillet and others (2022) and use a lower criterion of two times. In addition, we define a speed-up event as a surge candidate if the velocity is maintained above the threshold for at least four consecutive months (120 days), as it prevents the false identification of seasonal speed-ups as surge events. In the next section, we provide more information on how this and the subsequent proposed thresholds are used to detect surges.

Substantial and spatially concentrated thickening near the glacier terminus We generally consider a glacier to be a candidate for surging if it presents substantial and spatially concentrated changes in surface elevation (over 1-10 years) at lower elevations (near the glacier terminus; see Section 3.2.3 for more details), as this deviates from recent trends in global glacier thinning and retreat (Hugonnet and others, 2021). Thus, our objective is to identify glaciers that exhibited a substantial and widespread surface elevation gain (dynamical thickening) over the receiving zone. We consider clear statistical breakpoints (defined by a unitless changepoint score) and positive trends in surface elevation time series over glaciers to be the result of surge-induced dynamical thickening.

Abrupt changes in glacier surface crevassing Surges typically result in intense and widespread surface crevassing and changes in the crevasse patterns at the glacier surface (Truffer and others, 2021;

Guillet and others, 2022; Kääb and others, 2023). Such changes are identifiable via proxy as abrupt change points in glacier SAR backscatter trend time series (Leclercq and others, 2021; Kääb and others, 2023). Again, we consider clear statistical breakpoints (defined by a unitless change point score) and positive changes in trend of SAR backscatter time series over glaciers to be indicative of intense surface crevassing associated with a surge.

In the present surge identification scheme, we require at least two of the aforementioned criteria to be met in order to verify a detected event as a surge. As an example, an event flagged as a surge candidate through extended positive surface elevation but for which no signal is detected in either surface velocity or crevassing changes will not be classified as a surge. Adopting a multi-criteria approach makes the framework conservative, but this is necessary as it reduces the occurrence of false positives, such as significant accelerations in ice flow resulting from dynamic adjustment of tidewater glaciers to major calving events or frontal collapses (De Angelis and Skvarca, 2003; Benn and others, 2007; Benn and Evans, 2014). Although surges often result in an advance of the glacier terminus, not all surge-type glaciers show a terminal advance during the active phase (Murray and others, 1998; Benn and Evans, 2014; Guillet and others, 2022), and thus we do not use glacier advance as a criterion for surge identification.

3 Methods and data

Building upon the methodology developed by Guillet and others (2022), we propose a surge identification scheme that detects surge-type behaviour from abrupt variations in glacier surface velocity, positive changes in thickness and SAR backscatter.

3.1 Data

3.1.1 Surface velocity

Guillet and others (2022) relied on changes in annual NASA MEaSUREs ITS_LIVE surface velocity composite products (Gardner and others, 2024) to identify surges. Although this approach offered an efficient first step in automated surge identification, the annual resolution precluded the accurate identification of the timing of surge onset and termination. Here, we have used the entire archive of 120-m resolution ITS_LIVE feature-tracking velocity magnitude products prepared from individual pairs of Landsat, Sentinel-1 and Sentinel-2 images (Gardner and others, 2024), which has allowed the precise identification of the onset date, termination date, and duration of each surge.

3.1.2 Surface elevation changes

To detect positive thickness change anomalies (see Section 3.2.3), we used surface elevation time series prepared from Digital Elevation Models (DEMs) generated using stereo images acquired by the ASTER (Hugonnet and others, 2021) and Maxar WorldView-1/2/3 and GeoEye-1 satellite instruments (ArcticDEM, Porter and others (2018)). In their study, Hugonnet and others (2021) rely on a multistep outlier filtering approach to iteratively improve DEM quality by 1) removing elevation outliers using a reference elevation (TanDEM-X) and 2) filtering elevations that would lead to glacier thinning rates beyond the maxima defined by the authors. Although they subsequently used Gaussian process (GP) regression alongside iterative sigma-clipping to compute glacier surface elevation time series, recent efforts have discussed how this step likely results in filtering out the dynamic thickening signal for certain surge events (Guillet and Bolch, 2023). In the present study, we thus only rely on the TanDEM-X filtered surface elevation time series, omitting any of the Gaussian process filtering performed by Hugonnet and others (2021), and rather use a custom Gaussian process providing a more robust kernel to transient changes; see Section 3.2.3.

3.1.3 SAR backscatter

To infer changes in surface crevassing, we used ESA Sentinel-1 SAR backscatter time series back to its earliest usable data in 2015. The Sentinel-1 mission is set to acquire backscatter data in preset illumination angles in recurring orbits, defined by relative orbit numbers, at one of two polarizations (vertical, VV; horizontal, HH; and optionally cross-polarizations HV/VH), with the choice of polarization varying around the globe depending on the predominant use-case. The acquisition strategy per location, i.e. which angle and polarization, has been relatively consistent since 2018, but underwent several revisions between 2015 and 2018. Consequently, establishing the longest consistent time series for every considered glacier requires care.

For each glacier flowline point, we examined all Ground Range Detected (GRD) Sentinel-1 SAR products available through Google Earth Engine to obtain the longest consistent time series. Consistency is only retained through assessing the same illumination angle (relative orbit number) and polarization, so each combination of these were split up, and the longest combination was chosen per glacier. The GRD products in Google Earth Engine are not radiometrically corrected, meaning the reflective power is not normalized by distance and local incidence angle to the satellite. This is a problem when assessing absolute backscatter changes or comparing different relative orbits, but it should not introduce problems here

because we only measure relative changes through time for a set angle. As the SAR data are inherently noisy due to instrument noise and quasi-random speckle, we used time series sampled from medians in a 10 pixel (100 m) radius of each point.

3.1.4 ERA5-Land climate reanalysis data

ERA5 is a high-resolution, global climate reanalysis data set produced by the European Centre for Medium-Range Weather Forecasts (ECMWF) from 1950 to present (Muñoz-Sabater and others, 2021). ERA5-Land improves the spatial resolution of ERA5 reanalysis using a 9 km Gaussian grid (TCO1279) for the land surface level. The ERA5-Land data available through the Climate Data Store (Sabater, 2019) were re-gridded to a regular lat-lon grid of 0.1x0.1 degrees. The key atmospheric parameters used to run ERA5-Land are adjusted to compensate for the altitude discrepancies between the forcing grid and the higher resolution grid of ERA5-Land using lapse-rate correction (Muñoz-Sabater and others, 2021).

We analysed the 2-m air temperature and total precipitation variables from the monthly average ERA5-Land products between January 2000 to December 2023. We sampled the ERA5-Land products at the centroid of each RGI glacier polygon using bi-cubic interpolation.

3.1.5 Glacier outlines and flowlines

We used glacier outlines provided by the Randolph Glacier Inventory version 7.0 (RGI v7) (RGI 7.0 Consortium, 2023) and the released flowlines product available at <https://nsidc.org/data/nsidc-0770/versions/7>.

3.2 Detection of surge events

3.2.1 Data sampling strategy

Based on the spatial resolution of the ITS_LIVE and DEM products ($\approx 120\text{m}$), we limited our analysis to RGI glacier polygons with flowlines long enough to be sampled at ten equally spaced vertices, i.e longer than 20 pixels and 2.4 km. This results in a total of 32133 glaciers with 54178 flowlines, and thus 541780 points to automatically evaluate for surging (Figure 1).

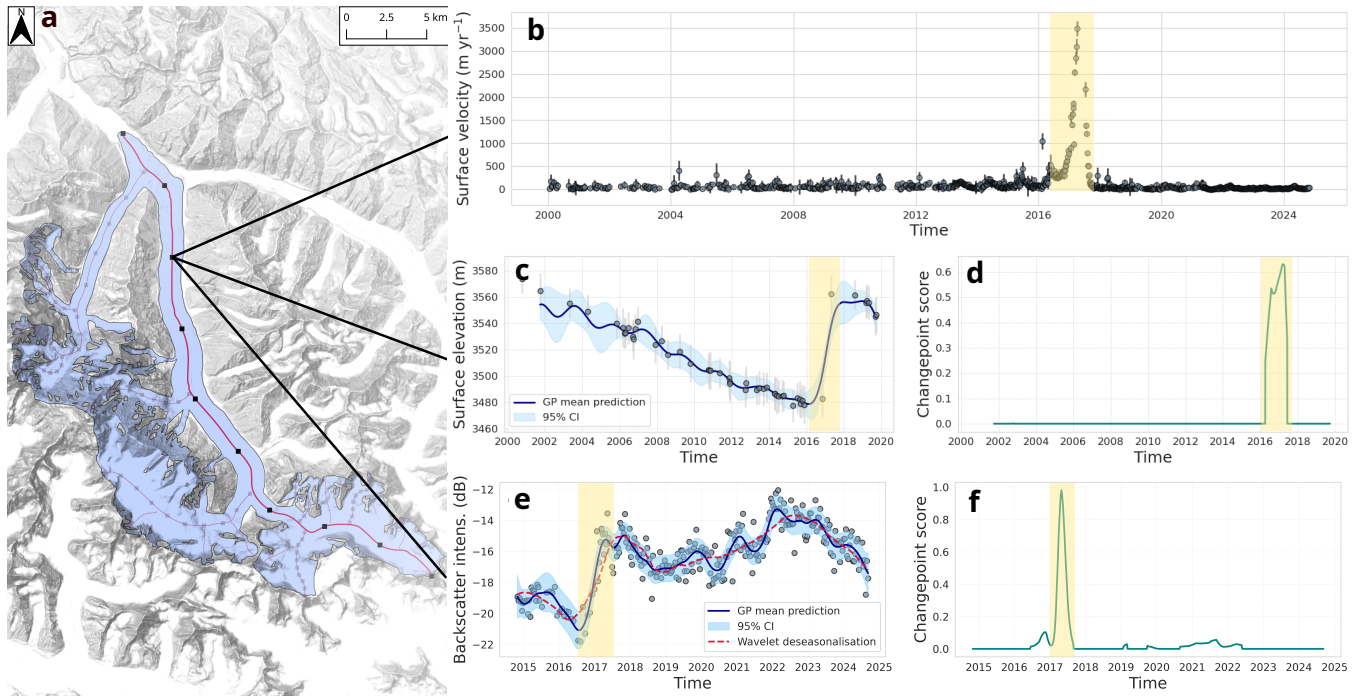


Fig. 1. Example of the data sampling strategy applied to Khurdopin glacier, Karakoram. **a)** The map shows the RGI7.0 outline of the glacier (blue area) as well as the different flowlines (greyed lines), with the main flowline highlighted in red. Black squares are vertices at which each dataset is sampled. **b)** ITS_LIVE surface velocity estimates. **c, d)** surface elevation change, and **e, f)** SAR backscatter. The scatterpoints in **c** and **e** represent the pre-Gaussian process regression time series. The mean of each Gaussian process regression is presented a solid blue line, while the shaded blue area is the 95% credible interval. **d, f)** Change point detection scores for the surface elevation change detection (**d**) and SAR backscatter (**f**) frameworks, see section 3.2.3. Note the variable x-axis ranges as the datasets span different periods. The synchronously detected surge in all three datasets is shaded in yellow.

3.2.2 Surface velocity

Automating the detection of glacier surge events within a time series of glacier surface velocity data faces challenges when relying solely on conventional signal processing techniques and time series analysis methodologies. Multiple sensors are used to prepare the ITS_LIVE velocity time series, which improves spatio-temporal sampling for all glaciers, but data quality issues arise due to the limitations of individual sensors, including cloud cover and illumination conditions for optical instruments. Such constraints lead to velocity data that have data gaps in time and space, with variable uncertainty, which presents difficulties for conventional time-series analysis methods meant for regularly sampled data. In addition, glacier surges demonstrate intricate dynamics, showing different velocity patterns with diverse durations, magnitudes, and temporal changes. Therefore, we chose a statistical modelling approach to automatically detect surges in the irregular surface velocity time series.

We apply the following framework independently to each point $s(x, y, z)$ along the flowline at which the velocity time series is sampled. We only consider surface velocity estimates computed with a temporal baseline of 6 to 110 days. We then normalise the surface velocity time series $U_s(t)$ using the mode of surface velocity magnitude for the full 2000-2024 time period. We assume that the observed surface velocity $U_s(t)$ is the result of two distinct sources: the baseline surface velocity of the glacier $U_b(t)$ and an "excess" surface velocity term $U_e(t)$ which potentially includes dynamic ice flow instabilities:

$$U_s(s, t) = U_b(s, t) + U_e(s, t) \quad (1)$$

Our surge identification scheme relies on estimating the excess velocity $U_e(t)$ at a given time t by modelling $U_b(t)$.

Several approaches to model time-varying glacier surface velocity have been proposed. However, these efforts rely on a periodic structure of the velocity signal (sine or cosine), often use higher-order polynomials to interpolate missing values, and/or require continuous temporal data coverage (e.g. Vijay and others, 2019; Greene and others, 2020; Charrier and others, 2022). Here, we model $U_b(s, t)$ for each point s of the flowline as a Gaussian process:

$$U_b(t) \sim \mathcal{GP}(\mu_U(t), k(t, t')) \quad (2)$$

where $\mu_U(t)$ is the time-dependent mean and $k(t, t')$ is the kernel function that captures the temporal covariance between data points.

Gaussian process mean The Gaussian process proposed here acts as a surrogate model, or emulator, for what can be considered the baseline surface velocity of each glacier. Thus, its mean represents the most likely baseline velocity value at any given time t and is derived directly from the data. Since the distributions of glacier surface velocity values are non-symmetric and present heavy positive tails, the median value for the full 2000–2024 period is not a robust estimate of the most probable baseline velocity value. Here we use the mode of the distribution of the surface velocity values as the mean for the Gaussian process. To calculate the mode of the distribution, we first used a Gaussian kernel to estimate the probability density function of the whole sample of glacier surface velocities. The mode was then estimated as the minimum of the negative probability density function. It is thus assumed that surges are represented by a relatively small proportion of the distribution and hence that the glacier is, more often than not, in quiescence during the 2000–2024 period.

Gaussian process covariance In practice, we model the changes in glacier velocity at a given point $s(x, y, z)$ and time t as a stochastically driven damped simple harmonic oscillator (SHO). This allows us to more intuitively capture potential variations in the frequency of baseline glacier surface velocity from one year to another. We use the `celerite2` (Foreman-Mackey and others, 2017) Python implementation of Gaussian process models with SHO kernel terms defined by the authors through the power spectral density (ω):

$$S(\omega) = \sqrt{\frac{2}{\pi}} \frac{S_0 \omega_0^4}{(\omega^2 - \omega_0^2)^2 + \omega_0^2 \omega^2 / Q^2} \quad (3)$$

with ω_0 being the undamped angular frequency and Q the quality factor describing the resonance of the harmonic oscillator. `celerite2` proposes an alternative parametrization of the SHO term and further allows the user to define more intuitive kernel hyperparameters of the form:

$$\rho = 2\pi/\omega_0, \text{ the undamped period of the oscillator (in days)} \quad (4)$$

$$\tau = 2Q/\omega_0, \text{ the damping timescale of the process (in days)} \quad (5)$$

$$\sigma = \sqrt{S_0 \omega_0 Q}, \text{ the standard deviation of the process (normalized)} \quad (6)$$

We thus define the covariance function as a sum of two SHO terms capturing velocity variations through an additive model as a annual and sub-annual (typically 4 months) periodic deviations:

$$k(t, t') = \underbrace{\text{SHO}(\rho = 365, \tau = 365 * 2, \sigma = \text{IPR}(U_s))}_{\text{Annual variations term}} + \underbrace{\text{SHO}(\rho = 365/4, \tau = 365, \sigma = \text{IPR}(U_s))}_{\text{Sub-annual variations term}} \quad (7)$$

where IPR represents the interpercentile range (between the 5th and 95th percentiles) of the entire available sample of glacier surface velocity measurements, U_s .

Using our fully-specified Gaussian process model (Equations 2 and 7), we can now derive an estimate of $U_b(s, t)$ through Gaussian Process regression for each sampling point s , and hence rewrite Equation 1 to estimate the excess velocity at a given time t (Figure 2):

$$U_e(s, t) = U_s(s, t) - U_b(s, t) \quad (8)$$

3.2.3 Surface elevation changes and SAR backscatter

We aim to identify glaciers that exhibited a substantial and widespread reorganisation of their surface as clear identifiers of a surge. This entails drastic increases in surface elevation gain (thickening) in their receiving zone in contrast to the expected glacier thinning trends (Hugonnet and others, 2021), or drastic changes in surface crevassing, as visible on backscatter time series (Leclercq and others, 2021; Kääb and others, 2023).

In practice, we are specifically aiming at detecting sharp transitions in trends in surface elevation change rates, as well as backscatter, as shown on Figure 1. Surface elevation change and SAR backscatter time series present similar structures in that they can be modelled as a trend term and one, or several, periodic terms (shown for elevation change in Hugonnet and others, 2021). However, they both present individual challenges which prevent the sole use of standard signal processing methodologies. Surface elevation change time series are plagued by their overall sparsity and irregular sampling, and SAR backscatter time series contain seasonal variations (largely due to precipitation and melt) with greater amplitudes than the typical change in trend from a surge that we wish to detect. Both existing data gaps, and high-amplitude periodic oscillations hamper the use of conventional trend change detection methods. We therefore set up a multistep framework to detect positive break points from both datasets. Similarly to section 3.2.2, the following framework is identical for each vertex $s(x, y, z)$ along the flowline at which the surface elevation and

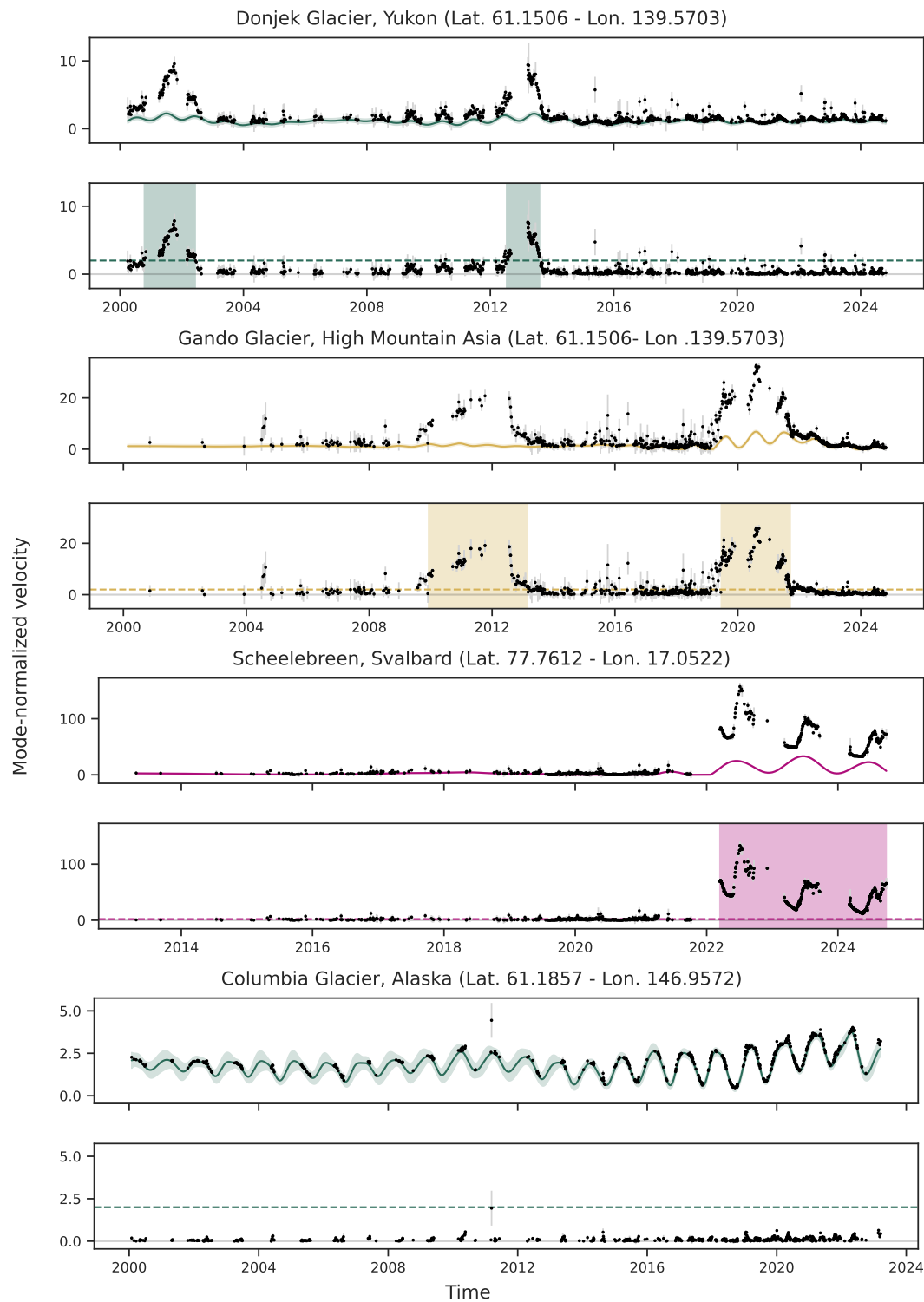


Fig. 2. Time series of ITS_LIVE glacier surface velocity estimates (black dots) for a vertex along the main flowline of selected glaciers. For each glacier the top plot presents ITS_LIVE glacier surface velocity estimate (black dots) and the computed baseline velocity (solid coloured curves, mean of the Gaussian process prediction), the shaded area is the 90% confidence interval. The bottom one presents the excess velocity estimates, i.e. the residuals from the Gaussian process regression (black dots), and automatically identified surge events (shaded regions). Columbia glacier is not a surging glacier and is presently used to demonstrate the proficiency of the Gaussian process in emulating glacier surface velocities.

backscatter time series are sampled.

Gaussian process regression and signal resampling We begin by modelling each time series $y(t)$ as a realisation of a Gaussian process:

$$y(t) \sim \mathcal{GP}(\mu_y(t), k(t, t')) \quad (9)$$

We again rely on `celerite2`'s `SHOTerm` (Eq. 3) to capture both the periodic structure of the signal, as well as longer-term (typically close to 5 years) trend:

$$k(t, t') = \underbrace{\text{SHO}(\rho = 365, \tau = 365 * \theta_1, \sigma = \text{IPR}(y))}_{\text{Annual variations term}} + \underbrace{\text{SHO}(\rho = 365 * \theta_2, \tau = 365, \sigma = \text{IPR}(y))}_{\text{Long-term trend term}} \quad (10)$$

where IPR represents the interpercentile range (between the 5th and 95th percentiles) of the entire available sample of either glacier surface elevation or backscatter measurements, y . θ_1 and θ_2 are parameters used to capture the wide diversity of surface elevation and backscatter patterns observed globally. They are fitted to each individual time series (from each flowline vertex) through maximum likelihood estimation using an L-BFGS scheme. Examples of realizations of individual Gaussian processes used for regression and interpolation of surface elevation and backscatter time series are given in panels b and d of Figure 1.

After fitting the Gaussian process model, each signal is resampled uniformly to ensure consistent spacing for subsequent analyses. This step minimises the risk of aliasing and ensures that our changepoint detection operates on an evenly sampled input signal.

Wavelet decomposition In order to identify changes in signal trend, each resampled GP estimate needs to be decomposed into multiple time scales, accounting for trend and seasonality. In practice, we here want to isolate the trend in either measurement by filtering out any high-amplitude seasonal signal. Since the resampled GP signal is not purely periodic, we perform signal decomposition using discrete wavelet transform with Daubechies 4 (db4) wavelets. We choose Daubechies wavelets as they are effective for capturing both transient features and structural changes in signals. The wavelet transform represents the signal $y(t)$ as a sum of approximations and details (Mallat, 1999):

$$y(t) = \sum_{j,k} c_{j,k} \psi_{j,k}(t), \quad (11)$$

where $\psi_{j,k}(t)$ are wavelet basis functions indexed by scale j and position k , and $c_{j,k}$ are the corresponding wavelet coefficients. An example of wavelet deseasonalisation is given in panel b and d of Figure 1.

Penalized changepoint detection We consider $y(t = k)$ to be a changepoint if at time $k \in \mathcal{T} = \{t_1, \dots, t_K\}_{K \leq T}$, there is a change in the mean value of the wavelet-decomposed GP estimate. We note \mathcal{T} a partition of the input signal $y(t)$ with $K + 1$ subsequences, where K is the number of changepoints. In our case, K is unknown but is assumed to be in the range $[0, 1]$ and is found through a changepoint detection procedure.

A changepoint detection procedure aims to find the optimal segmentation $\hat{\mathcal{T}}$ by minimising the quantitative criterion $V(\mathcal{T}, y) = \sum_{k=0}^K c(y_{t_k \dots t_{k+1}})$, with $c(\cdot)$ a cost function measuring, for each point $y(t = k)$ a changepoint partitioning precision; *i.e.* how well the signal is divided into segments such that each segment exhibits consistent statistical properties, with changepoints marking significant shifts in data characteristics. Finding $\hat{\mathcal{T}}$ is a discrete optimization problem, with, in our case, an unknown number of K changepoints and written as follows :

$$\min_{\mathcal{T}} V(\mathcal{T}, y) + \text{pen}(\mathcal{T}) = \min_{\mathcal{T}} \tilde{V}(\mathcal{T}, y) \quad (12)$$

with $\text{pen}(\mathcal{T})$ constraining the number of detected changepoints by effectively penalising models with a higher number of changepoints. The proposed changepoint detection procedure is implemented using `ruptures` (Truong and others, 2020) and made up of 3 main parts:

- (i) A search method or detection algorithm, to estimate $\hat{\mathcal{T}}$: we use the window search detection method, consisting of computing the discrepancy between two adjacent sliding windows along $y(t)$ (Truong and others, 2020).
- (ii) A constraint on the number of changepoints. In practice, we find that a penalisation parameter of 70 ensures the detection of a minimal number of changepoints in most cases.
- (iii) A cost function $c(\cdot)$. We use an ensemble of three different cost functions : a rank-based cost function (Lung-Yut-Fong and others, 2011), a Mahalanobis-type metric (Truong and others, 2019), and a kernelized mean change (Arlot and others, 2019).

Similarly to Katser and others (2021) we then rely on the aggregation of all models, combining different cost functions, to produce an aggregated cost; a method also known as "mixture of experts" by the machine learning community. For each model and cost function, a score quantifies how well a particular segmentation

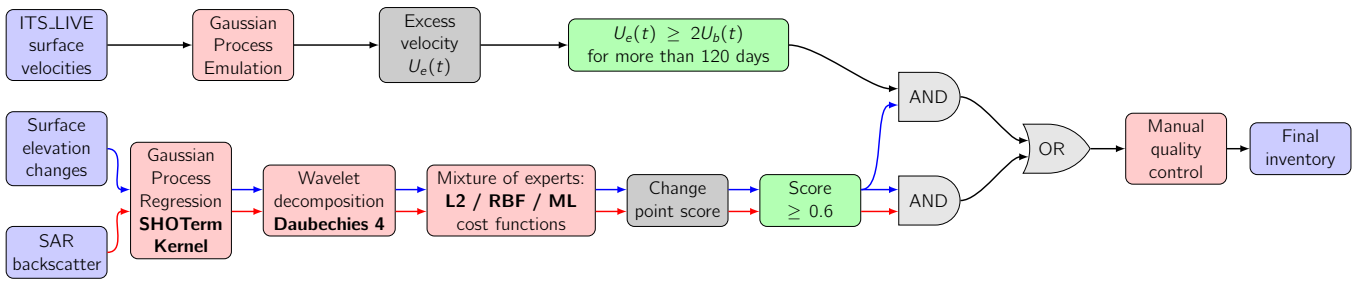


Fig. 3. Dataflow diagram overview of the surge event detection scheme, showing the flow of information between input and outputs (blue blocks), internally used data (white blocks), and processing steps (rounded blocks). Green blocks represent the data-specific surge detection thresholds described in Section 2. Blue and red arrows represent the dataflow of surface elevation and SAR backscatter measurements respectively. The blocks defined as AND and OR are logical gates, stipulating that surges have to be detected by either i) the surface elevation change and velocities detection schemes or ii) the surface elevation change and backscatter detection schemes.

fits the data. Scores are then scaled between 0 and 1 aggregated by taking the pointwise minimum. Since we are only interested in increases in the trend of the surface elevation change and SAR backscatter signals, we set the score of changepoints detected with a negative trend gradient to 0. Finally, vertices with a combined changepoint score greater than 0.6 are considered candidates for surging.

3.2.4 Combination of criteria and derivation of a surge inventory

Each of the aforementioned detection steps and data types lead to a different subset of candidate surge events (Figure 3). The subsets of potential surge-type glaciers are then compared based on their RGI v7.0 identification number. Sub-inventories are then combined as follows: glaciers detected by both our surface elevation change and surface velocity frameworks, or both the surface elevation change and SAR backscatter frameworks are considered to be surging (Figure 3). Since surge-induced changes in SAR backscatter are the result of changes in surface velocity, we do not consider the combination between our surface velocity and SAR backscatter frameworks to be indicative of surging, as other phenomena could be falsely identified as surges.

3.2.5 Validation and quality control

Validating the semi-automated detection of glacier surges is not straightforward due to existing inventories being derived from inconsistent methods and data sets. The most comprehensive inventory of surge-type glaciers is the one presented by Sevestre and Benn (2015). However, we argue that, due to the mismatch in the 2000-2024 period of our inventory and the 1861-2013 period of the Sevestre and Benn (2015) inventory, as well as the conceptual differences in the identification of surges, a detailed comparison between the two

inventories would be inconclusive. The most recent global inventory of glacier surges was presented by Kääb and others (2023) and relied on the visual interpretation of Sentinel-1 backscatter signals, following the methods described in Leclercq and others (2021).

We rely on the inventory of Kääb and others (2023) as a validation data set and assess the capability of our detection framework quantitatively through the use of the Jaccard index, also known as the Intersection over Union, a similarity measure commonly used in object detection and expressed as follows:

$$J(A, B) = \frac{|A \cap B|}{|A \cup B|} = \frac{|A \cap B|}{|A| + |B| - |A \cap B|} \quad (13)$$

where A and B represent two different sets of glaciers: A , a validation set of surge-type glaciers identified and B , the glaciers with semi-automatically detected surge events identified in this study. $|A \cap B|$ thus represents the total surface area (in km²) covered by the glaciers identified in both A and B , while $|A \cup B|$ is the surface area covered by the sum of A and B . The Jaccard index is thus bounded between 0 and 1, with a value of 0 when the sets are completely dissimilar and 1 if the sets are identical.

In addition to the proposed validation experiment, each identified glacier has been manually checked following the criteria proposed in Section 2. In the final product, potential misidentifications have been culled.

4 Results and discussion

4.1 Global distribution of glaciers with active surges between 2000 and 2024

Of the ≈ 32000 glaciers analysed, we detected 246 glaciers with active surges over the 2000 to 2024 period (Figure 4). Most glaciers surged only once, while five glaciers surged two or more times between 2000 and 2024, and one glacier surging four times (Sit'Kusa/Turner glacier, Alaska). Compared to version 7 of the RGI, in Alaska and the Yukon, we identify one surge on a glacier that was previously classified as "No evidence" (Nadina Glacier), as well as 4 previously classified as "Probable" surge-type (Martin River, Marvine, Valerie, and Ferris glaciers). In Svalbard, we note a surge of Lilliehöökreen, previously classified as having no evidence of surge-type behaviour. We further identified nascent surges at Nordssyselbreen, Aavatsmarkbreen and Doktorbreen, all classified as "Probable" surge type. Similarly, we identify a surge on Borebreen, classified as "Possible" surge-type. We finally report the onset of surges at Deltabreen and Seftrombreen which, according to Sevestre and Benn (2015), have not surged in the 20th century, effectively

displaying quiescence for the past 165 and 128 years, respectively. All other identified surges in our global sample affect previously identified surge-type glaciers.

Glaciers with active surges during the 2000-2024 period represent around 1% of all glaciers studied and 0.1% of all glaciers in RGI V7.0. However, the total surface area of these glaciers with active surges is approximately 38000 km², which corresponds to approximately 5.5% of the worldwide glacierized area outside of the polar ice sheets.

The spatial distribution of surge events is consistent with previous assessments. Approximately 167 (68%) glaciers with identified surges are located in High Mountain Asia, with 78 (32%) in the circum-Arctic region (the Arctic Ring). Within the Arctic Ring, Alaska-Yukon and Svalbard-Russian Arctic had the highest number of glaciers with active surges, with estimates of 28 and 24, respectively. Our method identified 16 active surge-type glaciers in Greenland, 12 in the Canadian Arctic, and one in the Andes. No surge events were detected during the 2000-2024 period in Iceland. A near or total absence of surges in Iceland is expected (Kääb and others, 2023), as most known surge-type glaciers in Iceland surged during the 1990s (Hannesdóttir and others, 2020) and are therefore likely to be quiescent (Björnsson and others, 2003) or senescent (Benn and others, 2023).

4.2 Climatic controls on the distribution of surge-type glaciers

Surge-type glaciers are found within a specific climatic envelope where they are accompanied by non-surge-type glaciers; beyond this envelope, only non-surge-type glaciers are typically observed. Figure 5 shows the distribution of non-surge-type and surge-type glaciers in relation to the median temperature and the median total annual precipitation from ERA5-Land data for the period between 1990 to 2024. The surge-type glacier climatic envelope typically encompasses a median annual temperature of -1 to -20° C and a median total precipitation of 100 to 1200 mm a⁻¹ (Figure 5, panel a).

Seasonal climate data reveal additional insights on surge-type glacier distributions (Figure 5, panels b and c). Surge-type glaciers typically occur over a broad range of median total winter (October-April for the Northern Hemisphere, June-September for the Southern Hemisphere) precipitation (20 to 1000 mm a⁻¹) and median winter temperature (-10 to -30° C), while they are still absent from either end of the ranges for the larger population of global glaciers. The occurrence of surge-type glaciers is firmly bound by median summer temperature, as surge-type glaciers are almost non-existent in regions where the median summer temperature exceeds 3 ° C. Similarly, 90% of the surge-type glacier population lies within a median total

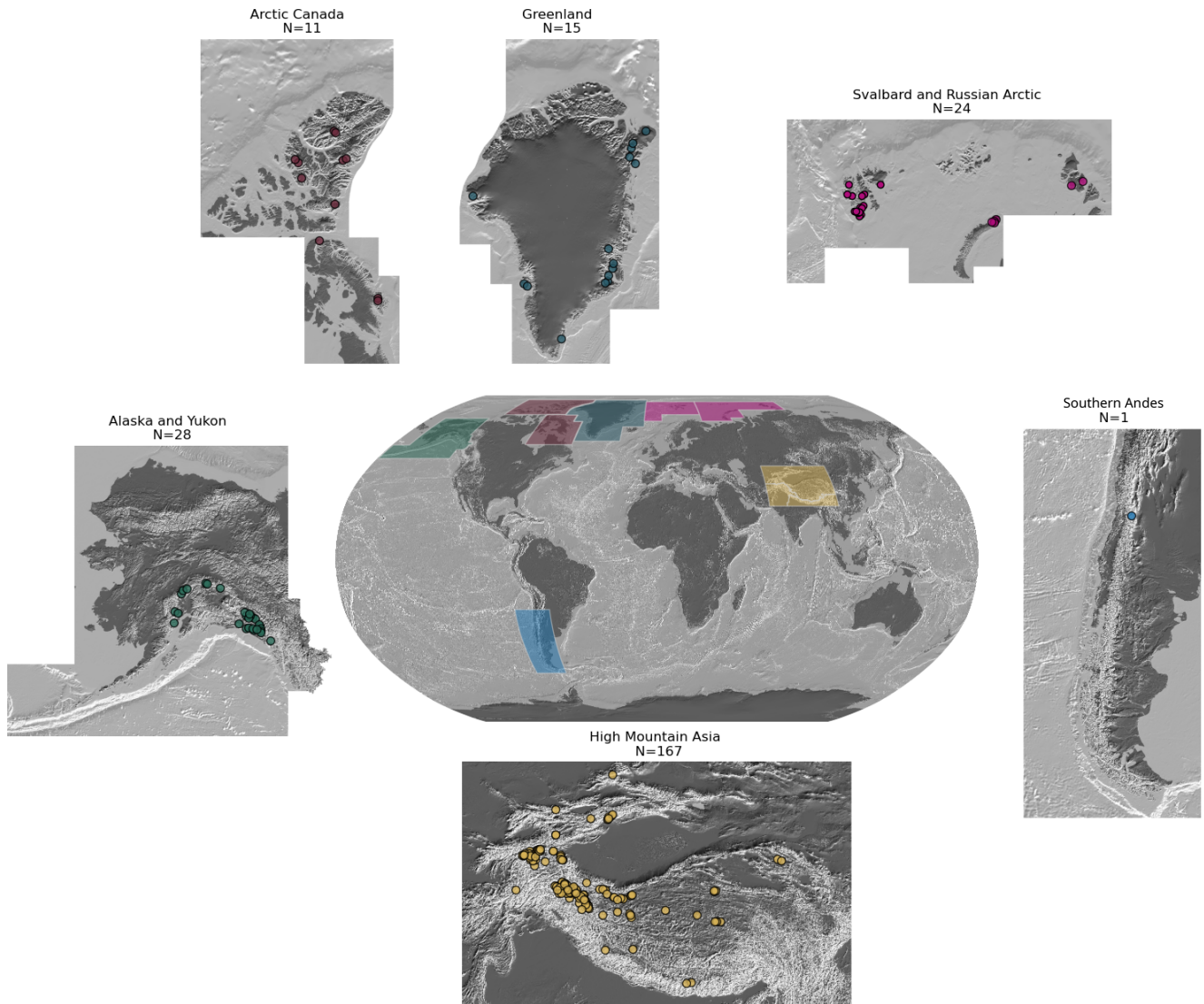


Fig. 4. Global distribution of 246 glaciers with active surges between 2000 and 2024 identified with our methodology. Prominent but well-known clusters of surge-type glaciers are evident in High Mountain Asia and the Arctic Ring. N refers to the number of surge-type glaciers detected.

summer precipitation range of 100-1000 mm a⁻¹.

The clearest climatic relationship used to distinguish surge-type glaciers is between the median summer temperature and the median total winter precipitation (Figure 6). Surge-type glaciers are absent beyond median summer temperatures higher than 3 ° C and less than -10 ° C. Similarly, they are seldom present in regions where the median total winter precipitation exceeds 1000 mm a⁻¹.

The characteristics of the climatic envelope established by our analyses are similar to those of Sevestre and Benn (2015) and in very strong agreement with the envelope described by Lovell and others (2023) using ERA5-Land. Using the glaciers identified by Sevestre and Benn (2015), Falaschi and others (2018), Guillet and others (2022) Lovell and others (2023), and Kääb and others (2023), we calculated an updated climate envelope using the more modern ERA5-Land products, which very strongly concurs with our results (Figures 6 and 5).

We finally focus on further validating the proposed climatic envelope. We here aim at avoiding sampling bias in climatic distributions, resulting from sample size differences between non surge-type (around 270000 glaciers) and surge-type glaciers. For the latter, we use both the 246 surge-type glaciers from this study, as well as the composite inventory formed from the datasets of Sevestre and Benn (2015), Falaschi and others (2018), Guillet and others (2022) Lovell and others (2023), and Kääb and others (2023), containing close to 2200 glaciers. From each sample of glaciers, we obtain continuous estimate probability density functions (PDFs) on the number of glaciers in a given temperature/precipitation range by kernel density estimation, using a Gaussian kernel. Figure 7 represents 200000 samples drawn from each PDF and highlights the clustering of surge-type glaciers within the defined climatic envelope. The samples derived from the proposed inventory (Figure 7, panel a) show a greater variance compared to those from the composite inventory (Figure 7, panel b), which results from initial sample size disparity.

4.3 Surge event statistics

The following section describes surge events statistics that are solely derived from velocity time series. Due to the data quality issues described in Section 4.6.1, velocity time series for glaciers in the polar regions lack the temporal resolution necessary to clearly identify surge onset and termination dates. Consequently, we do not consider the surges identified in the Canadian Arctic and the periphery of Greenland within the present section.

The peak surface velocity is defined here as the maximum velocity measured over all sampled ITS_LIVE

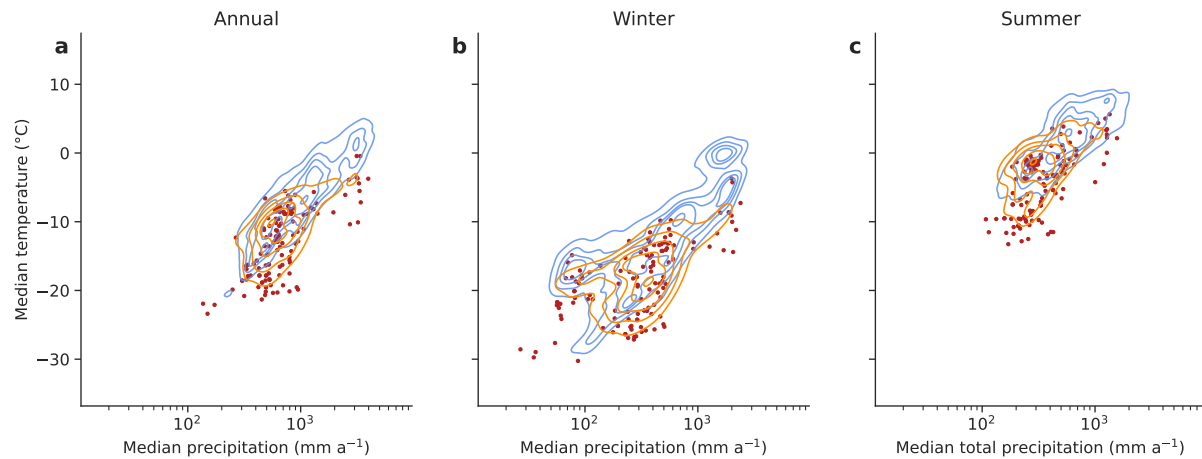


Fig. 5. Median temperature and total precipitation for surge-type (orange) and non-surge-type glaciers (blue). **a, b, c)** Due to the disparity in sample size between surge-type (246) and non-surge-type glaciers (more than 270000), the median temperature/median total precipitation relationship is represented using a kernel density estimate, all levels represent lines of probability, or density of the 2D distributions: 20%, 40%, 60%, 90% and 99%. **a)** Median total annual precipitation versus median annual temperature. **b)** Median total winter precipitation versus median winter temperature. **c)** Median total summer precipitation versus median summer temperature. Distribution of surge-type glaciers from this study (red scatter plots) and using the glaciers identified by Sevestre and Benn (2015), Falaschi and others (2018), Guillet and others (2022) Lovell and others (2023), and Käab and others (2023) (orange kernel density estimate).

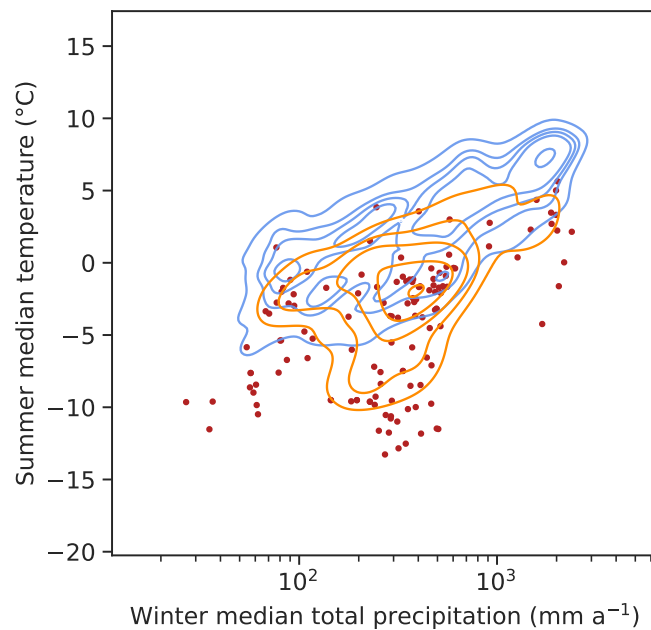


Fig. 6. Median summer temperature and median total winter precipitation for surging and non-surge-type glaciers. Distribution of surge-type glaciers from this study (red scatter plots) and using the glaciers identified by Sevestre and Benn (2015), Falaschi and others (2018), Guillet and others (2022) Lovell and others (2023), and Käab and others (2023) (orange kernel density estimate). Lines represent different density levels : 30%, 50%, 70%, 90% and 99%. Also note the difference in median summer temperature between surge-type and non-surge type glaciers.

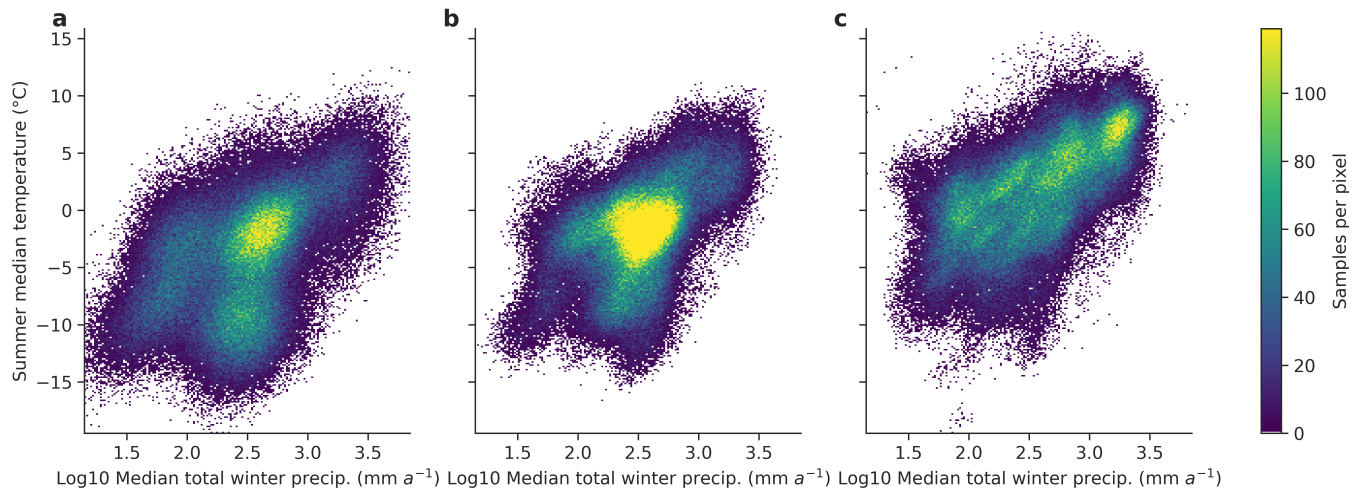


Fig. 7. Median summer temperature and median total winter precipitation for **a**) surge-type glaciers from this study, **b**) the surge-type glaciers from by Sevestre and Benn (2015), Falaschi and others (2018), Guillet and others (2022) Lovell and others (2023), and Kääb and others (2023) and **c**) non-surge-type glaciers from the RGI v7.0. Note the important clustering of surge-type glaciers within the defined climatic envelope in **a** and **b**. Non-surge type glaciers are more uniformly distributed over the temperature/precipitation spectrum.

time series. Similarly the surge duration is taken as the longest time interval for which the glacier is detected to be actively surging, for all individual surges and across all flowline vertices. The distributions of the peak surge velocity and duration for 193 surge events are presented in Figure 8.

4.3.1 Peak surface velocity during surges

The median peak surface velocity for the entire sample is 4.2 m day^{-1} , with an interpercentile range of 2.1 m day^{-1} (Figure 8a). The glacier displaying the highest peak surge surface velocity is that of Sít' Kusa in Alaska, where the peak velocity reached an estimate of $28.8 \pm 0.4 \text{ m day}^{-1}$.

A closer analysis of regional samples shows a marked similarity between Alaska-Yukon and Svalbard-Russian Arctic. The median peak surface velocities are 6.8 and 6.5 m day^{-1} , while interpercentile ranges are 6.2 and 5.4 m day^{-1} . Surges in High Mountain Asia present significantly lower peak surface velocities, with a median value of 3.3 m day^{-1} and an interpercentile range of 2.2 m day^{-1} .

4.3.2 Duration

Across 193 surge events detected between 2000 and 2024, the median surge duration was 2.6 years, with an interquartile range (25th to 75th percentile) of 2.1 years. While the median surge duration for Alaska-Yukon is 2.3 years, surges appear to last longer in Svalbard-Russian Arctic and High Mountain Asia with median durations of 3.3 and 2.8 years respectively. In addition, surge durations for the Alaska-Yukon sub-

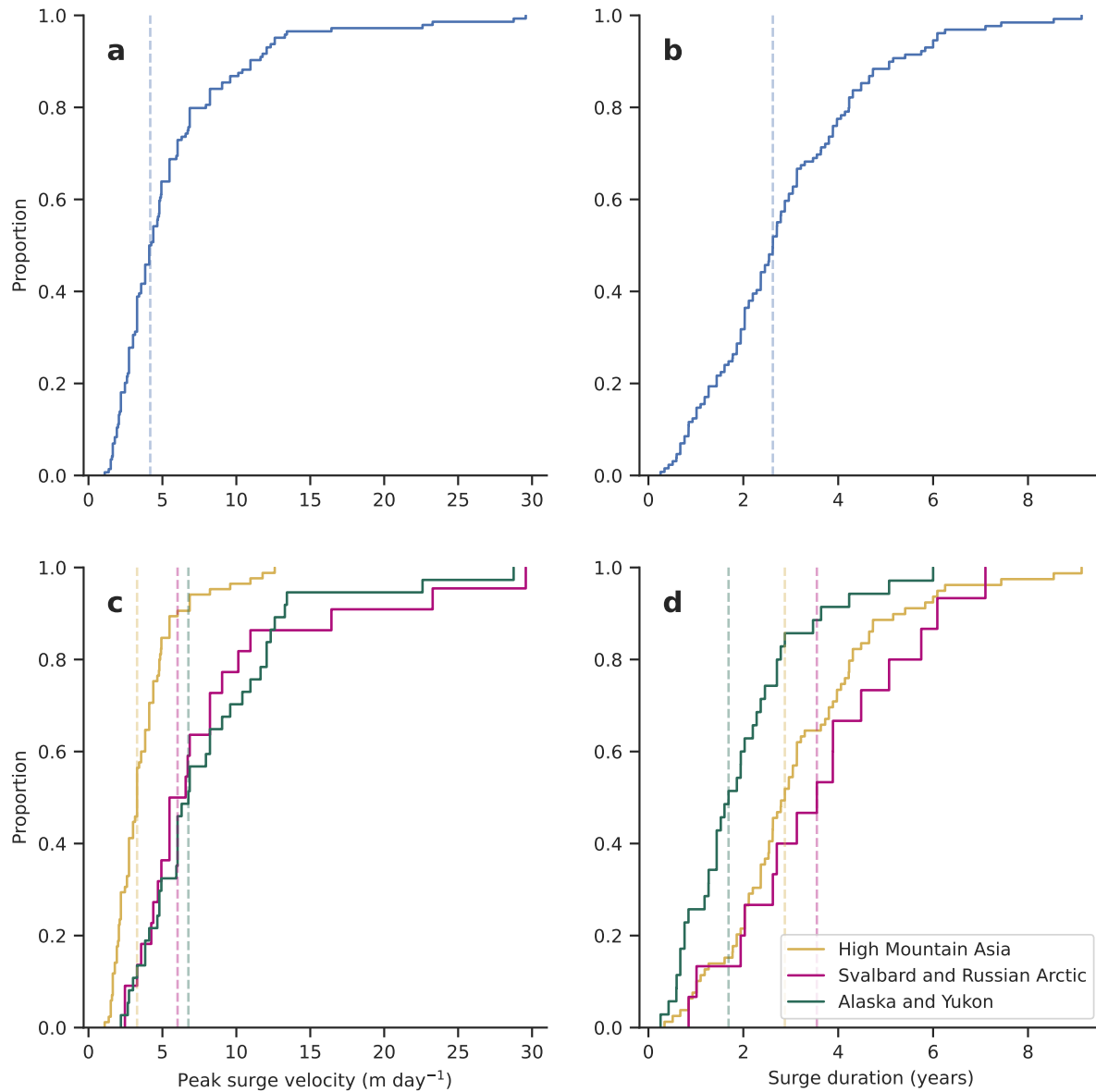


Fig. 8. Empirical cumulative distributions of **a)** peak surface velocity and **b)** surge duration, for the full sample of detected surge events. Regional distributions of **c)** peak surface velocity and **d)** surge duration for Alaska-Yukon, High Mountain Asia, and Svalbard-Russian Arctic. Vertical dashed lines are the median of each distribution.

cluster present a slightly narrower interpercentile range (1.7 years) compared to Svalbard-Russian Arctic (2.6 years) and High Mountain Asia (2.1). The longest detected surge event is the 9.1 year surge of West Kunlun Glacier (RGI2000-v7.0-G-13-47689) in the Western Kunlun between 2008 and 2019. In Alaska-Yukon, the longest surge is that of Klutlan Glacier (St. Elias Mountains, Yukon) which lasted 6.8 years. In Svalbard-Russian Arctic, the longest surge is the still-ongoing 12 year surge of Austfonna Basin-3.

Further analyses showed no linear correlation between peak surface velocity and the duration of individual surge events. In addition, no linear correlation has been found between surge duration, peak surface velocity and glacier geometry (length, surface area and surface slope) i.e. longer and/or steeper glaciers do not appear to be more prone to faster or longer-lasting surges.

4.4 Regional differences in surge dynamics: on the Svalbard vs Alaska-type classification

The hydrological switch (Alaska-type surges) hypothesis posits relatively short active phases, typically lasting between 1 and 3 years, and reaching a peak velocity of 10 to 100 metres per day (Murray and others, 2003). Conversely, the thermal switch hypothesis supposes longer durations than Alaska-type surges, typically lasting up to more than 10 years and reaching peak velocity between 1 and 15 metres per day (Murray and others, 2003). We therefore test for the existence of statistical differences between the distributions of peak surface velocity and surge duration between different surge clusters, with a focus on Alaska-Yukon and Svalbard-Russian Arctic.

The distribution of peak velocity during surge events appears similar in both regions, with surge events reaching more than 20 m day⁻¹ of peak velocity and both distributions displaying a median close to 6 m day⁻¹, with an average spread of 5 m day⁻¹. More quantitatively, a two-sample Kolmogorov-Smirnov test comparing the distributions of peak surface velocity for surges in Alaska-Yukon and Svalbard-Russian Arctic return a statistic of 0.18 and a p-value of 0.81 indicating that the two distributions are not significantly different. Our results therefore do not statistically support a Svalbard-vs-Alaska-type classification. This finding corroborates the idea of dynamical unity between what was previously considered two ends of a behavioural spectrum resulting from distinct processes (Jiskoot, 2011; Herreid and Truffer, 2016; Sevestre and Benn, 2015; Benn and others, 2019a).

A closer investigation of the differences between glaciers in Alaska-Yukon, Svalbard-Russian Arctic and High Mountain Asia further reveals the breadth of dynamical behaviours displayed by surges.

First, it is worth noting that we expect the distributions described in Section 4.3 to be updated by future work as, out of the 31 surges detected in Svalbard-Russian Arctic, the onset and termination date could only be estimated for 18 of them. Most ongoing surges have already lasted longer than the estimated median surge duration in Svalbard-Russian Arctic and are likely to further positively skew the distribution. As an example, the surge of the Nathorstbreen Glacier system, the onset of which is invisible on ITS_LIVE, is believed to have occurred around 2006 (Sund and others, 2014). Similarly, the surges of Austfonna Basin-3 and Scheelebreen, which started in 2012 and 2021, respectively, are still ongoing.

Second, to understand the regional differences in surge dynamics, we find added value in investigating the velocity signals from individual surges. Figure 9 shows the similarities between the surface velocity signals for Alaska-Yukon and High Mountain Asia, as well as how they differ from surges in Svalbard-Russian Arctic. The acceleration phases of all the surges presented in Figure 9 first shows relatively low linear increase in surface flow velocity, before a rapid switch to a quasi-exponential regime roughly 500 days prior to reaching peak value (Figure 9 panels 13, 26, 39). All three clusters further seem to reach around 10% of maximum velocity value. Individual differences are apparent in the transition between slow linear flow acceleration and active surge phase. In the selected surges from Alaska-Yukon, few glaciers, apart from Donjek and Lowell (Figure 9 3, 8), show notable increases in surface flow earlier than 500 days prior to the peak. This dynamic is similar in Svalbard-Russian Arctic, where only Monacobreen ice cap (Figure 9, 18) shows a gradual increase in ice flow before a dramatic spike in velocity, marking the transition to an active surge phase.

Notable differences between regions are further observable in the deceleration phase of individual surges. Surges in the Alaska-Yukon cluster show a median deceleration to 10% of the maximum surface velocity within 180 days of their peak. In addition, most glaciers in the sample are back to quiescent velocity 500 days after peak. In the Svalbard-Russian Arctic cluster, surging velocities are maintained at 50% of the maximum surface velocity for 180 days. Most deceleration phases last for than 1000 days, with Negribreen and Sonklarbreen still close to 20% of peak surface velocity 2000 days after (Figure 9 15, 21). Surges in High Mountain Asia typically show a more symmetric velocity profile, centred around the date of peak velocity. We observe a median deceleration to around 30% of the maximum surface velocity at 180 days after peak, with most surges terminated by day 800. In addition, slowdown phases for surges in Svalbard-Russian Arctic show very strong seasonal fluctuations, that are mostly absent from in Alaska-Yukon and High Mountain Asia.

We interpret the regional differences in surge duration as different sensitivities of individual glaciers to the propagation of a frictional instability at the glacier bed. Glaciers such as Kluane, Arnesenbreen, or RGI2000-v7.0-G-13-05693 (Figure 9 panels 5, 14, 30) show a very clear spike in surface velocity, without gradual flow acceleration before the transition point. This testifies to the rapid onset of transient feedbacks between drainage and friction (Benn and others, 2019b; Thøgersen and others, 2024). For surges with a more gradual onset such as Donjek, Osbornbreen and Gulyia ice cap (Figure 9 panels 3, 16, 27), lower enthalpy production likely first leads to the observable gradual increase in ice flow. The glacier then transitions to a velocity weakening regime (Thøgersen and others, 2024), as increased sliding velocity leads to lower basal friction triggering a sliding/frictional heating feedback (Benn and others, 2023), further enhancing glacier motion and propagating the surge.

We further infer longer deceleration phases in Svalbard-Russian Arctic, as well as the drastic seasonal speed-ups, to be correlated to the large proportion of tidewater surge-type glaciers in the region (Figure 10). Indeed, contrarily to High Mountain Asia where all surge-type glaciers are land-terminating, or Alaska-Yukon where only Sit'Kusa (Turner), Valerie and La Prouse glaciers are marine-terminating, all but one of the identified surge-type glaciers in Svalbard-Russian Arctic are tidewater glaciers. The surge detected at Vallåkrabreen, the only land-terminating glacier in our Svalbard-Russian Arctic sample, displays a velocity signal similar to surges affecting land-terminating glaciers in Alaska-Yukon and High Mountain Asia. We however want to note that 3 of the tidewater glaciers in our sample, Sit'Kusa (Alaska-Yukon), Arnesenbreen (Svalbard-Russian Arctic) and Sortebræ (East Greenland), present velocity signals closer to that of land-terminating glaciers. While the surge Sortebræ still displays a strong periodicity, Arnesenbreen and Sit'Kusa only multiple surges over the studied time period. We did not find any correlation between glacier geometry as given in the version 7 of the RGI (mostly length, area, altitude range and slope) and either the maximum velocity or duration of surge events. We cannot control for differences in thermal regime between land-terminating and tidewater-glaciers, or in our sample. We thus posit that ice-ocean interactions at the front of surging tidewater glaciers lead to the observed longer active phases in the Svalbard-Russian Arctic cluster. More specifically, higher hydrostatic pressure at the glacier terminus likely hampers frontal drainage of the water at the glacier bed resulting in the inability of basal drainage systems to act as efficient enthalpy sinks (e.g. Terleth and others, 2024). This ultimately leads to a more gradual termination of surges (Benn and others, 2019b, 2023) and higher sensitivity to seasonal meltwater input. The interpretation of our results therefore corroborates the hypothesis that surge termination is

controlled by how efficiently the drainage system can evacuate the basal enthalpy (Benn and others, 2019a; Ravier and others, 2023; Thøgersen and others, 2024; Terleth and others, 2024).

The presented differences in surge peak surface velocity and duration distributions between Alaska-Yukon, Svalbard-Russian Arctic and High Mountain Asia reflect variations in enthalpy budgets. While individual variations might originate from different enthalpy producers, such as changes in a glacier's thermal regime or mass balance, poor basal drainage or rapid influx of meltwater, they do not represent any fundamental contrast in surge mechanism and rather form a wide spectrum of dynamical behaviours.

4.5 Evaluation of inter-inventory consistency

We now attempt to quantify the similarity between our catalogue of surge events and that of Kääb and others (2023) for global detection as well as Koch and others (2023), solely for Svalbard. It is important to note that we rely only on surges that Kääb and others (2023) classify as certain.

For this experiment, we first focus on Svalbard, for which ITS_LIVE surface velocity estimates are only reliably available from 2013, effectively reducing the mismatch in the periods considered between the inventories from Kääb and others (2023) and Koch and others (2023) and the one proposed here. Between the proposed inventory and that of Kääb and others (2023), the Jaccard index estimate for Svalbard gives an acceptable similarity between the sets of glaciers with a result of 0.61. This is due to the presence of four relatively large glaciers in Kääb and others (2023), which are not captured by either the surface velocity or the SAR backscatter scheme. When comparing our results to the Svalbard inventory of Koch and others (2023), the Jaccard index quantifies a good similarity with a result of 0.71. The difference between our inventory and that of Koch and others (2023) first lies in the detection of a surge on Austfonna Basin-3, which, while surging, currently undergoes linear deceleration with marked seasonal accelerations. Second, Koch and others (2023) describe a 2017 surge of Orsabreen, which is invisible in the three datasets we analysed, and not reported in Kääb and others (2023).

In High Mountain Asia, we choose to study the regional Jaccard index for the two main clusters of surge-type glaciers in High Mountain Asia: Pamir range/Tibetan Plateau (RGI region 13) and the Karakoram Range (region 14). In the Pamirs and Tibetan Plateau, we obtain a Jaccard index of 0.58, similar to that of Svalbard. The similarity is greater in the Karakoram, where the Jaccard index is 0.81. Finally, in Alaska (region 01), the similarity index is 0.67.

Upon further investigation, false-negatives originated from our surface velocity identification scheme

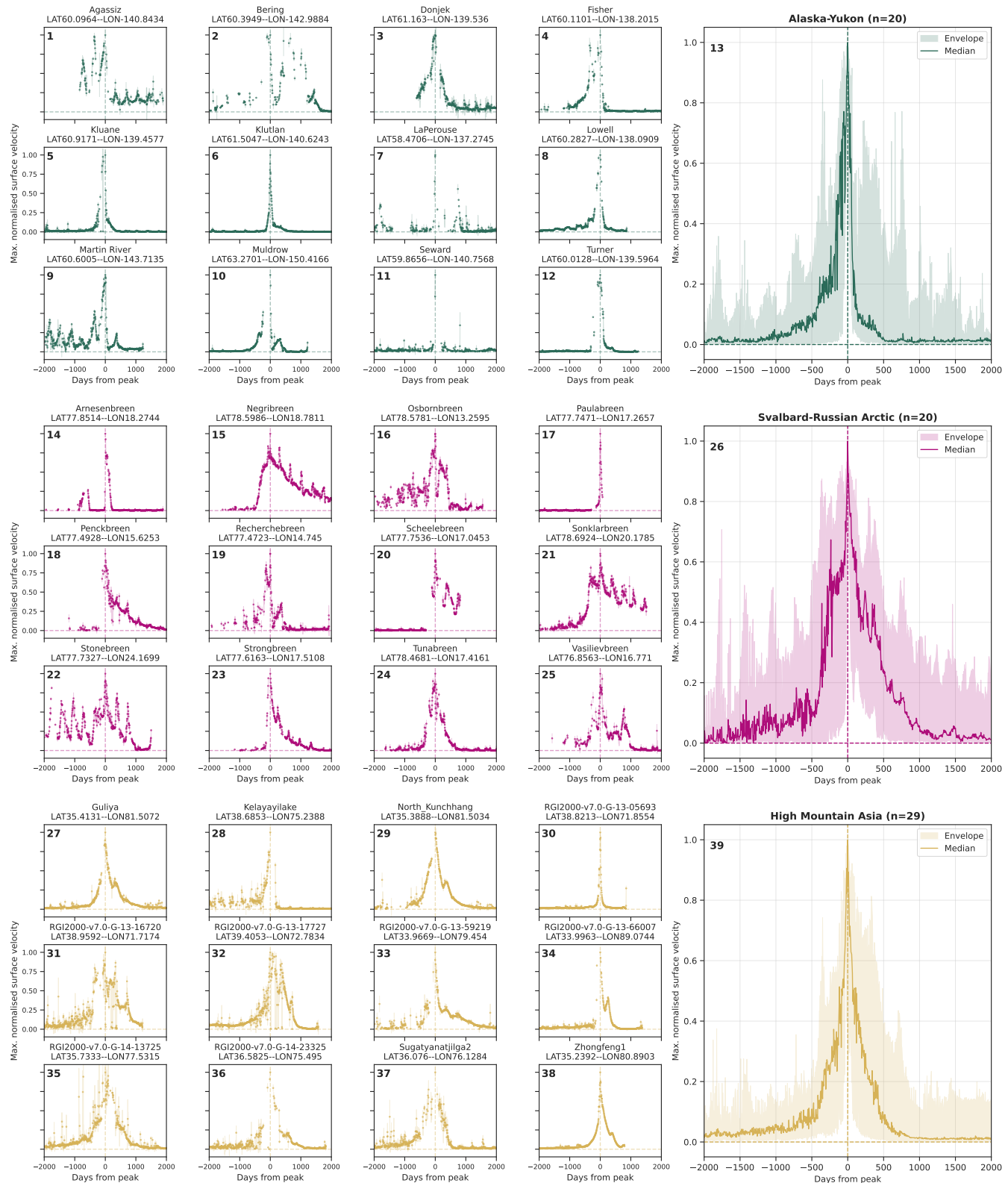


Fig. 9. Example of ITS_LIVE surface velocity times for surge events in **1-12)** Alaska-Yukon, **14-25)** Svalbard-Russian Arctic, and **27-38)** High Mountain Asia. **13, 26, 39)** Regional stacks of surface velocity time series. Bold lines represent stack median and shaded areas cover the minimum to maximum range. Subtitles list the name/RGI identification number of each glacier as well as the sampling location of each surface velocity time series. The x-axes are centred on the reference date when peak velocity was reached for each event, and y-axes show the maximum-normalised surface velocity.

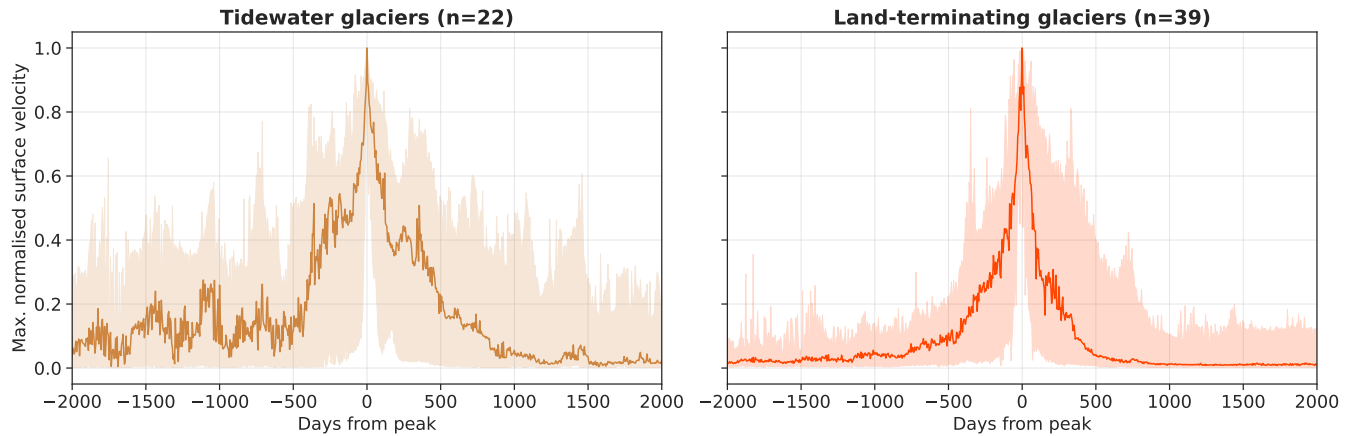


Fig. 10. Stacks of surface velocity time series for glacier from all clusters, by terminus type. Bold lines represent stack median and shaded areas cover the minimum to maximum range. The x-axes are centred on the reference date when peak velocity was reached for each event, and y-axes show the maximum-normalised surface velocity. N specifies the number of time-series used to generate each subplot. Time-series were sampled across clusters, only accounting for terminus type. Note the strong periodic component of the velocity signal for tidewater glaciers, as well as the overall greater variance in surface flow velocities.

lead to several points of discussion. First, in some rare cases, the quiescent behaviour of the given glacier is obscured as the glacier is surging over the whole considered period, preventing the computation of reliable baseline behavior. Second, the glacier is already decelerating at the beginning of the time series, and hence, there are no positive anomalies to be detected (Austfonna Basin-3 and Nathorstbreen glacier system in Svalbard, for example). Data availability and quality problems (RGI2000-v7.0-G-13-16640, RGI2000-v7.0-G-14-08450, etc.) obscure potential surges; a point further discussed in Section 4.6.1. Missed detections from the SAR backscatter and surface elevation change scheme are a direct consequence of our changepoint detection threshold, which is purposely conservative to avoid false positives. Finally, in Alaska, the difference between our inventory and Kääb and others (2023) is a result of their non-detection of the surges of the three lobes forming the Sít' Tlein (Malaspina - RGI2000-v7.0-G-01-15261) glacier system. We however want to mention that Kääb and others (2023) identify the propagation on an instability on the Seward lobe of Sít' Tlein glacier but classify it as uncertain.

4.6 Towards a fully automated detection of glacier surges: uncertainties, challenges, and perspectives

4.6.1 Uncertainties with the current inventory

Here, we reiterate that the suggested catalogue of surge events cannot be expected to be exhaustive. Given our strict multi-criteria identification framework, we believe the likelihood of false positives to be

minimal. However, the likelihood of false negatives is significantly higher, as shown by the comparably low number of detected surges, compared to even regional inventories (e.g. Guillet and others, 2022; Guo and others, 2023). The relatively coarse spatial resolution of all the data products significantly hinders the detection of surges on small valley glaciers. Limitations in data availability and quality further hinder, for example, the recognition of surges prior to the deployment of Landsat-8 (2013) in Svalbard (e.g. the pre-2013 surge initiations of Comfortlessbreen and Blomstrandbreen, Sund and Eiken, 2010) and some regions of the Tibetan Plateau (glacier CN5Z514H0005 – RGI2000-v7.0-G-13-60066, for example, Guillet and others, 2022), since the ITS_LIVE archive only includes data after April 2013. Given that most of the ITS_LIVE measurements have been derived from optical imagery (either Landsat or Sentinel-2), the polar night further obstructs the detection of surge events in the Greenland periphery and the high Arctic regions. Although the exact number is unknown, ITS_LIVE data quality issues lead to the non-detection of an important number surges on smaller valley glaciers in the Pamirs, Karakoram and Tibetan Plateau (Guillet and others, 2022). As a specific example, the ongoing surge of Nadina Glacier in Alaska is invisible in both ITS_LIVE and SAR backscatter timeseries, while the dynamical thickening and advance of the glacier terminus are clearly visible from very high resolution imagery. Similar problems arise for DEMs derived from optical instruments, in addition to the general sparsity of DEM time series. In Svalbard, the 2019 surge of Sonklarbreen is not visible in the elevation data while it is detected through the excess velocity and SAR backscatter schemes.

A final data-related source of false negatives lies in the vector layers used to sample each time series. We indeed identified several cases of surges from individual former tributaries of larger glacier systems, where the surge-related terminus advance leads to the reconnection of the tributary with the main glacier trunk. In these cases, the surging tributary effectively advances past the boundary of the RGI polygon and the dynamical thickening signal, if present, can only be detected on the main trunk. Similarly, we identified surges initiating close to the glacier terminus, where the dynamical thickening signal is only identifiable outside of the considered vector layers (polygon and/or flowline), effectively rendering the detection impossible.

Finally, our method of identifying surges depends on empirical thresholds in order to distinguish between baseline and surge-type behaviour of a given glacier. By expressing intuitive thresholds, we aim to maintain transparency in our methodology and advocate for a clear explanation of the reasoning behind our threshold choice. The surface velocity threshold is intentionally set to detect surges at the lower end of

the surge magnitude spectrum, while the changepoint detection threshold used for both surface elevation and backscatter time series is purposely conservative. Although relying solely on thresholding could result in extended false identifications due to data quality, we have implemented additional spatio-temporal constraints (minimum duration of an event, etc.) within the surge identification process before manually culling any potential remaining misidentification. Consequently, we are confident that our multi-criteria surge identification method is robust and can reliably determine if a particular glacier is experiencing a surge at a specific time, given the available data and thresholds. We however want to state here that glaciers typically affected by slow (e.g. Frappé and Clarke, 2007; Flowers and others, 2011), or long-lasting (i.e. more than several decades long) surges, such as Airdrop Glacier in the Canadian Arctic (Lauzon and others, 2023), cannot be expected to be detected by the proposed methodology.

4.6.2 Perspectives

We anticipate that the limitations of glacier velocity fields derived from optical methods will become less significant in the future, thanks to the expansion of archives from synthetic aperture-radar imaging satellite missions such as the European Space Agency Sentinel-1 (Lemos and others, 2018; Zhu and others, 2021), and the NASA-ISRO Synthetic Aperture Radar (NISAR) mission (Kellogg and others, 2020). We also believe that there is untapped potential in the addition of other diagnostic criteria in future efforts (Guillet and others, 2022), such as the use of Landsat imagery to generate time series of glacier terminus position change (Vale and others, 2021), debris displacement (Herreid and Truffer, 2016), as well as spatio-temporal changes in glacier surface characteristics through direct mapping of crevasses (Herzfeld and Zahner, 2001; Bhardwaj and others, 2016).

In this work, we showed that the complexity and diversity in surge-type behaviour can be captured in part by straightforward statistical models. In addition, we highlighted that our methods cannot outperform human expertise in identifying surges, a point similarly expressed by Kääb and others (2023). Simple statistical models lack a holistic perspective of surges as a glacier-wide destabilisation and the ability to detect subtle shifts in patterns that can hardly be described by quantitative thresholds. An example of this is the terminal advance of a significant number of glaciers during their respective surges which, while clearly visible on the SAR backscatter images (Leclercq and others, 2021; Kääb and others, 2023), would require adding an entirely new model to the existing framework to be captured adequately (Herreid and Truffer, 2016; Vale and others, 2021). Recent deep learning-based image segmentation techniques (e.g. Xie

and others, 2020; Maslov and others, 2024), operating in higher-dimensional spaces and leveraging entire data archives, present an exciting prospect towards the fully automated detection of surge events.

5 Conclusions

We have developed a semi-automated framework to identify surge events using remote sensing observations from the 2000 to 2024 period. We demonstrated the potential for Gaussian processes to act as a surrogate statistical model, or emulator, for baseline surface glacier velocity. By extracting the modelled baseline behaviour from point-wise glacier surface velocity time series, we were able to detect dates of surge onset and termination, as well as important quantitative information such as peak velocity for every identified surge event. We finally used a changepoint detection procedure to identify surge-related changes in glacier thickness and surface characteristics from surface elevation and SAR backscatter time series. By combining potential surges identified from surface elevation changes with 1) candidate surges from ITS_LIVE and 2) candidate surges from SAR backscatter time series, we are confident in the robustness of the present inventory, up to a level of uncertainty allowed by the relatively coarse resolution of the considered data products. The resulting surge event inventory is thus conservative and not exhaustive, as there are numerous false negatives that cannot effectively be captured by our methodology.

In total, we identified 246 glaciers with active surges during the 2000-2024 period. The vast majority of surge-type glaciers are located in two already well-known clusters: High Mountain Asia (167) and the Arctic Ring (78, Alaska-Yukon, Arctic Canada, Greenland, Svalbard-Russian Arctic).

We evaluated our inventory of glaciers with detected surge events against existing inventories covering similar time periods but different surge identification schemes. We found a broadly good agreement between our results and the reference dataset in all considered areas.

Using the generated surge event catalogue, we tested several predictions of the enthalpy balance theory. Analysing the ERA-5 Land data, we first validated the presence of an optimal climatic envelope, bounded both by temperature and precipitation, where surges are most probable. Surge-type glaciers are absent above a threshold median summer temperature higher than 3 °C and lower than -10 °C. In addition, they are seldom found in regions where the median total winter precipitation exceeds 1000 mm a⁻¹. Then, focusing on Svalbard-Russian Arctic and Alaska-Yukon, we showed the limits of the predictive capabilities of the hypothesis of surges being either hydrologically or thermally controlled, fortifying the enthalpy balance theory as a unifying framework with which to study surges. We thus suggest that the community

moves away from classifying surge events as being either "Alaska-type" or "Svalbard-type" since it does not adequately capture the range of observed behaviours, and instead consider their dynamic unity. We explored why surges affecting Svalbard-Russian Arctic glaciers typically last longer than those in Alaska-Yukon, emphasising the importance of glacier terminus type. Furthermore, we proposed that, in these regions, surges impacting tidewater glaciers endure longer than those that affect land-terminating glaciers due to a reduced hydrostatic gradient, which limits efficient drainage of the glacier bed. However, further research is needed to control for other differences between these glaciers (e.g. glacier thermal regime).

Finally, we here reiterate that our resulting inventory cannot be expected to be exhaustive. However, this work does not need to be static and we invite the community to build on the present efforts by incorporating further past and future surges detected through different, yet consistent, schemes relying on newer datasets and additional identification criteria.

Acknowledgements

GG was supported by NASA awards 80NSSC24K1633 and 80NSSC20K1595, NSF award 1917536 and ERC Advanced Grant 'Past and Future High-resolution Global Glacier Mass Changes (GLACMASS)' - 101096057 DS was supported by NASA awards 80NSSC24K1633 and 80NSSC20K1595. We thank Editor in Chief Hester Jiskoot, Harold Lovell, and one anonymous reviewer for their careful reading of our manuscript and their very constructive comments. We thank Martin Truffer, Regine Hock, Andy Aschwanden, and Charlie Raymond for their comments and constructive remarks throughout this work.

Author contribution

GG was the main coordinator of the study, which initiated from original ideas by GG and DB. GG designed the statistical models and implemented the code, with input from DS and RH. GG performed all data analyses and made the figures in close collaboration with DB, OK, ESM and DS, with additional input from RH. RH generated and provided the surface elevation data. ESM generated and provided the SAR backscatter data. OK curated the inventory with input from GG. GG, OK, DB and ESM interpreted the results. GG wrote the original manuscript with major text contributions from OK, DS, DB and ESM. RH, DB and ESM provided extensive text reviews and edits.

Data

All velocity, elevation, SAR backscatter, climate reanalysis, and Randolph Glacier Inventory datasets used in this paper are freely available from the respective data providers listed in Section 3.1 Data. The surge event catalogue is available here : https://github.com/gregguillet/surge_events_catalogue

References

- Arlot S, Celisse A and Harchaoui Z (2019) A kernel multiple change-point algorithm via model selection. *Journal of Machine Learning Research*, **20**(162), 1–56
- Bazai NA, Cui P, Liu D, Carling PA, Wang H, Zhang G, Li Y and Hassan J (2022) Glacier surging controls glacier lake formation and outburst floods: The example of the Khurdopin Glacier, Karakoram. *Global and Planetary Change*, **208**, 103710
- Benn D and Evans DJ (2014) *Glaciers and glaciation*. Routledge, London, second edition
- Benn DI (2021) Surging glaciers in Scotland. *Scottish Geographical Journal*, **137**(1-4), 1–40 (doi: 10.1080/14702541.2021.1922738)
- Benn DI, Warren CR and Mottram RH (2007) Calving processes and the dynamics of calving glaciers. *Earth-Science Reviews*, **82**(3-4), 143–179
- Benn DI, Fowler AC, Hewitt I and Sevestre H (2019a) A general theory of glacier surges. *Journal of Glaciology*, **65**(253), 701–716 (doi: 10.1017/jog.2019.62)
- Benn DI, Jones RL, Luckman A, Fürst JJ, Hewitt I and Sommer C (2019b) Mass and enthalpy budget evolution during the surge of a polythermal glacier: A test of theory. *Journal of Glaciology*, **65**(253), 717–731 (doi: 10.1017/jog.2019.63)
- Benn DI, Hewitt IJ and Luckman AJ (2023) Enthalpy balance theory unifies diverse glacier surge behaviour. *Annals of Glaciology*, **63**(8789), 8894 (doi: 10.1017/aog.2023.23)
- Bhambri R, Hewitt K, Kawishwar P and Pratap B (2017) Surge-type and surge-modified glaciers in the Karakoram. *Scientific reports*, **7**(1), 15391
- Bhardwaj A, Sam L, Singh S and Kumar R (2016) Automated detection and temporal monitoring of crevasses using remote sensing and their implications for glacier dynamics. *Annals of Glaciology*, **57**(71), 81–91
- Björnsson H, Pálsson F, Sigurdsson O and Flowers GE (2003) Surges of glaciers in Iceland. *Annals of glaciology*, **36**, 82–90

- Charrier L, Yan Y, Trouvé E, Koeniguer EC, Mouginot J and Millan R (2022) Fusion of multitemporal multisensor velocities using temporal closure of fractions of displacements. *IEEE Geoscience and Remote Sensing Letters*, **19**, 1–5
- Clarke GK (1976) Thermal regulation of glacier surging. *Journal of Glaciology*, **16**(74), 231–250
- Clarke GK, Collins SG and Thompson DE (1984) Flow, thermal structure, and subglacial conditions of a surge-type glacier. *Canadian Journal of Earth Sciences*, **21**(2), 232–240
- Cogley JG, Arendt AA, Bauder A, Braithwaite RJ, Hock R, Jansson P, Kaser G, Moller M, Nicholson L, Rasmussen LA and others (2010) Glossary of glacier mass balance and related terms
- Cuffey KM and Paterson WSB (2010) *The Physics of Glaciers*. Butterworth-Heinemann/Elsevier, 4th edition, ISBN 978-0-08-091912-6
- De Angelis H and Skvarca P (2003) Glacier surge after ice shelf collapse. *Science*, **299**(5612), 1560–1562
- Ding M, Huai B, Sun W, Wang Y, Zhang D, Guo X and Zhang T (2018) Surge-type glaciers in Karakoram Mountain and possible catastrophes alongside a portion of the Karakoram Highway. *Natural Hazards*, **90**(2), 1017–1020 (doi: 10.1007/s11069-017-3063-4)
- Falaschi D, Bolch T, Lenzano MG, Tadono T, Lo Vecchio A and Lenzano L (2018) New evidence of glacier surges in the central andes of argentina and chile. *Progress in Physical Geography: Earth and Environment*, **42**(6), 792–825
- Fatland DR and Lingle CS (2002) InSAR observations of the 1993–95 Bering Glacier (Alaska, USA) surge and a surge hypothesis. *Journal of Glaciology*, **48**(162), 439–451
- Flowers G, Roux N, Pimentel S and Schoof C (2011) Present dynamics and future prognosis of a slowly surging glacier. *The Cryosphere*, **5**(1), 299–313
- Foreman-Mackey D, Agol E, Ambikasaran S and Angus R (2017) Fast and Scalable Gaussian Process Modeling with Applications to Astronomical Time Series. *The Astronomical Journal*, **154**(6), 220 (doi: 10.3847/1538-3881/aa9332)
- Fowler A (1987) A theory of glacier surges. *Journal of Geophysical Research: Solid Earth*, **92**(B9), 9111–9120
- Fowler A, Murray T and Ng F (2001) Thermally controlled glacier surging. *Journal of Glaciology*, **47**(159), 527–538
- Frappé TP and Clarke GKC (2007) Slow surge of Trapridge Glacier, Yukon Territory, Canada. *Journal of Geophysical Research: Earth Surface*, **112**(F3) (doi: 10.1029/2006JF000607)
- Gao Y, Liu S, Qi M, Xie F, Wu K and Zhu Y (2021) Glacier-Related Hazards Along the International Karakoram Highway: Status and Future Perspectives. *Frontiers in Earth Science*, **9**

- Gardner AS, Fahnestock MA and Scambos TA (2024) ITS_LIVE Regional Glacier and Ice Sheet Surface Velocities. (NSIDC-0776, Version 1) (doi: 10.5067/6II6VW8LLWJ7), accessed: 2025-04-24
- Gilbert A, Leinss S, Kargel J, Kääb A, Gascoïn S, Leonard G, Berthier E, Karki A and Yao T (2018) Mechanisms leading to the 2016 giant twin glacier collapses, Aru Range, Tibet. *The Cryosphere*, **12**(9), 2883–2900
- Greene CA, Gardner AS and Andrews LC (2020) Detecting seasonal ice dynamics in satellite images. *The Cryosphere*, **14**(12), 4365–4378
- Guan W, Cao B, Pan B, Chen R, Shi M, Li K, Zhao X and Sun X (2022) Updated surge-type glacier inventory in the West Kunlun Mountains, Tibetan Plateau, and implications for glacier change. *Journal of Geophysical Research: Earth Surface*, **127**(1), e2021JF006369
- Guillet G and Bolch T (2023) Bayesian estimation of glacier surface elevation changes from DEMs. *Frontiers in Earth Science*, **11**, 1076732
- Guillet G, King O, Lv M, Ghuffar S, Benn D, Quincey D and Bolch T (2022) A regionally resolved inventory of High Mountain Asia surge-type glaciers, derived from a multi-factor remote sensing approach. *The Cryosphere*, **16**(2), 603–623 (doi: 10.5194/tc-16-603-2022)
- Guo L, Li J, Dehecq A, Li Z, Li X and Zhu J (2023) A new inventory of High Mountain Asia surging glaciers derived from multiple elevation datasets since the 1970s. *Earth System Science Data*, **15**(7), 2841–2861 (doi: 10.5194/essd-15-2841-2023)
- Hannesdóttir H, Sigurðsson O, Prastarson RH, Guðmundsson S, Belart J, Pálsson F, Magnússon E, Víkingsson S, Kaldal I and Jóhannesson T (2020) A national glacier inventory and variations in glacier extent in Iceland from the Little Ice Age maximum to 2019. *Jökull*, **12**, 1–34
- Heinrichs TA, Mayo LR, Trabant D and March R (1995) Observations of the surge-type Black Rapids Glacier, Alaska, during a quiescent period, 1970–92. Technical report, US Geological Survey
- Herreid S and Truffer M (2016) Automated detection of unstable glacier flow and a spectrum of speedup behavior in the Alaska Range. *Journal of Geophysical Research: Earth Surface*, **121**(1), 64–81 (doi: 10.1002/2015JF003502)
- Herzfeld UC and Zahner O (2001) A connectionist-geostatistical approach to automated image classification, applied to the analysis of crevasse patterns in surging ice. *Computers & geosciences*, **27**(5), 499–512
- Hugonnet R, McNabb R, Berthier E, Menounos B, Nuth C, Girod L, Farinotti D, Huss M, Dussailant I, Brun F and Kääb A (2021) Accelerated Global Glacier Mass Loss in the Early Twenty-First Century. *Nature*, **592**(7856), 726–731 (doi: 10.1038/s41586-021-03436-z)

- Humphrey N, Raymond C and Harrison W (1986) Discharges of Turbid Water during Mini-Surges of Variegated Glacier, Alaska, U.S.A. *Journal of Glaciology*, **32**(111), 195–207 (doi: 10.3189/S0022143000015513)
- Humphrey NF and Raymond CF (1994) Hydrology, erosion and sediment production in a surging glacier: Variegated Glacier, Alaska, 1982–83. *Journal of Glaciology*, **40**(136), 539–552 (doi: 10.3189/S0022143000012429)
- Jiskoot H (2011) Glacier surging. In VP Singh, P Singh & UK Haritashya (ed.), *Encyclopedia of Earth Sciences Series*, 415–428, Springer Netherlands
- Kääb A, Leinss S, Gilbert A, Bühler Y, Gascoïn S, Evans SG, Bartelt P, Berthier E, Brun F, Chao WA and others (2018) Massive collapse of two glaciers in western tibet in 2016 after surge-like instability. *Nature Geoscience*, **11**(2), 114–120
- Kääb A, Bazilova V, Leclercq PW, Mannerfelt ES and Strozzi T (2023) Global Clustering of Recent Glacier Surges from Radar Backscatter Data, 2017–2022. *Journal of Glaciology*, 1–9 (doi: 10.1017/jog.2023.35)
- Kamb B and Engelhardt H (1987) Waves of Accelerated Motion in a Glacier Approaching Surge: The Mini-Surges of Variegated Glacier, Alaska, U.S.A. *Journal of Glaciology*, **33**(113), 27–46 (doi: 10.3189/S0022143000005311)
- Kamb B, Raymond CF, Harrison WD, Engelhardt H, Echelmeyer KA, Humphrey N, Brugman MM and Pfeffer T (1985) Glacier Surge Mechanism: 1982–1983 Surge of Variegated Glacier, Alaska. *Science*, **227**(4686), 469–479 (doi: 10.1126/science.227.4686.469)
- Katser I, Kozitsin V, Lobachev V and Maksimov I (2021) Unsupervised offline changepoint detection ensembles. *Applied sciences*, **11**(9), 4280
- Kellogg K, Hoffman P, Standley S, Shaffer S, Rosen P, Edelstein W, Dunn C, Baker C, Barela P, Shen Y and others (2020) NASA-ISRO synthetic aperture radar (NISAR) mission. In *2020 IEEE Aerospace Conference*, 1–21, IEEE
- Koch M, Seehaus T, Friedl P and Braun M (2023) Automated Detection of Glacier Surges from Sentinel-1 Surface Velocity Time Series—An Example from Svalbard. *Remote Sensing*, **15**(6), 1545 (doi: 10.3390/rs15061545)
- Lauzon B, Copland L, Van Wychen W, Kochtitzky W and McNabb R (2023) Evolution of the dynamics of Airdrop Glacier, western Axel Heiberg Island, over a seven-decade-long advance. *Arctic Science*, **10**(1), 48–68
- Leclercq PW, Kääb A and Altena B (2021) Brief communication: Detection of glacier surge activity using cloud computing of Sentinel-1 radar data. *The Cryosphere*, **15**(10), 4901–4907
- Lei Y, Yao T, Tian L, Sheng Y, Lazhu, Liao J, Zhao H, Yang W, Yang K, Berthier E, Brun F, Gao Y, Zhu M and Wu G (2021) Response of downstream lakes to Aru glacier collapses on the western Tibetan Plateau. *The Cryosphere*, **15**(1), 199–214 (doi: 10.5194/tc-15-199-2021)

- Lemos A, Shepherd A, McMillan M, Hogg AE, Hatton E and Joughin I (2018) Ice velocity of Jakobshavn Isbræ, Petermann Glacier, Nioghalvfjerdsfjorden, and Zachariæ Isstrøm, 2015–2017, from Sentinel 1-a/b SAR imagery. *The Cryosphere*, **12**(6), 2087–2097
- Lingle CS and Fatland DR (2003) Does englacial water storage drive temperate glacier surges? *Annals of Glaciology*, **36**, 14–20
- Lovell H and Fleming EJ (2023) Structural evolution during a surge in the Paulabreen glacier system, Svalbard. *Journal of Glaciology*, **69**(273), 141–152 (doi: 10.1017/jog.2022.53)
- Lovell H, Carrivick JL, King O, Sutherland JL, Yde JC, Boston CM and Malecki J (2023) Surge-type glaciers in Kalaallit Nunaat (Greenland): distribution, temporal patterns and climatic controls. *Journal of Glaciology*, 1–18
- Lung-Yut-Fong A, Lévy-Leduc C and Cappé O (2011) Homogeneity and change-point detection tests for multivariate data using rank statistics. *arXiv preprint arXiv:1107.1971*
- Mallat S (1999) *A wavelet tour of signal processing*. Academic Press
- Maslov KA, Schellenberger T, Persello C and Stein A (2024) Glacier Mapping from Sentinel-1 SAR Time Series with Deep Learning in Svalbard. In *IGARSS 2024-2024 IEEE International Geoscience and Remote Sensing Symposium*, 14–17, IEEE
- Meier MF and Post A (1969) What are glacier surges? *Canadian Journal of Earth Sciences*, **6**(4), 807–817
- Merrand Y and Hallet B (1996) Water and sediment discharge from a large surging glacier: Bering Glacier, Alaska, U.S.A., summer 1994. *Annals of Glaciology*, **22**, 233–240 (doi: 10.3189/1996AoG22-1-233-240)
- Muhammad S, Li J, Steiner JF, Shrestha F, Shah GM, Berthier E, Guo L, Wu Lx and Tian L (2021) A holistic view of Shisper Glacier surge and outburst floods: from physical processes to downstream impacts. *Geomatics, Natural Hazards and Risk*, **12**(1), 2755–2775
- Muñoz-Sabater J, Dutra E, Agustí-Panareda A, Albergel C, Arduini G, Balsamo G, Boussetta S, Choulga M, Harrigan S, Hersbach H and others (2021) ERA5-Land: A state-of-the-art global reanalysis dataset for land applications. *Earth system science data*, **13**(9), 4349–4383
- Murray T and Porter PR (2001) Basal conditions beneath a soft-bedded polythermal surge-type glacier: Bakaninbreen, Svalbard. *Quaternary International*, **86**(1), 103–116
- Murray T, Dowdeswell JA, Drewry DJ and Frearson I (1998) Geometric evolution and ice dynamics during a surge of Bakaninbreen, Svalbard. *Journal of Glaciology*, **44**(147), 263–272

- Murray T, Strozzi T, Luckman A, Jiskoot H and Christakos P (2003) Is there a single surge mechanism? Contrasts in dynamics between glacier surges in Svalbard and other regions. *Journal of Geophysical Research: Solid Earth*, **108**(B5)
- Nolan M (2003) The Galloping Glacier trots: Decadal-scale speed oscillations within the quiescent phase. *Annals of Glaciology*, **36**, 7–13
- Paul F, Strozzi T, Schellenberger T and Käab A (2017) The 2015 surge of Hispar Glacier in the Karakoram. *Remote Sensing*, **9**(9), 888
- Porter C, Morin P, Howat I, Noh MJ, Bates B, Peterman K, Keeseey S, Schlenk M, Gardiner J, Tomko K, Willis M, Kelleher C, Cloutier M, Husby E, Foga S, Nakamura H, Platson M, Wethington J Michael, Williamson C, Bauer G, Enos J, Arnold G, Kramer W, Becker P, Doshi A, D'Souza C, Cummins P, Laurier F and Bojesen M (2018) ArcticDEM, Version 3 (doi: 10.7910/DVN/OHHUKH)
- Ravier É, Lelandais T, Vérité J and Bourgeois O (2023) Variations in hydraulic efficiency of the subglacial drainage landsystem control surging and streaming regimes of outlet glaciers. *Journal of Glaciology*, **69**(276), 860–878
- RGI 70 Consortium (2023) Randolph Glacier Inventory - A Dataset of Global Glacier Outlines, Version 7.0 (doi: 10.5067/f6jmovy5navz)
- Round V, Leinss S, Huss M, Haemmig C and Hajnsek I (2017) Surge dynamics and lake outbursts of Kyagar Glacier, Karakoram. *The Cryosphere*, **11**(2), 723–739
- Sabater JM (2019) ERA5-Land monthly averaged data from 1950 to present (doi: 10.24381/cds.68d2bb30), accessed on 14-Jun-2024
- Sevestre H and Benn DI (2015) Climatic and geometric controls on the global distribution of surge-type glaciers : Implications for a unifying model of surging. *Journal of Glaciology* (doi: 10.3189/2015JoG14J136)
- Solgaard A, Simonsen S, Grinsted A, Mottram R, Karlsson N, Hansen K, Kusk A and Sørensen L (2020) Hagen Bræ: A surging glacier in North Greenland 35 years of observations. *Geophysical Research Letters*, **47**(6), e2019GL085802
- Sund M and Eiken T (2010) Recent surges on Blomstrandbreen, Comfortlessbreen and Nathorstbreen, Svalbard. *Journal of Glaciology*, **56**(195), 182–184
- Sund M, Lauknes TR and Eiken T (2014) Surge dynamics in the Nathorstbreen glacier system, Svalbard. *The Cryosphere*, **8**(2), 623–638
- Terleth Y, Bartholomäus TC, Liu J, Beaud F, Mikesell TD and Enderlin EM (2024) Transient subglacial water routing efficiency modulates ice velocities prior to surge termination on SítKusá, Alaska. *Journal of Glaciology*, **70**, e29, 1–17 (doi: 10.1017/jog.2024.38)

- Thøgersen K, Gilbert A, Bouchayer C and Schuler TV (2024) Glacier surges controlled by the close interplay between subglacial friction and drainage. *Journal of Geophysical Research: Earth Surface*, **129**(10), e2023JF007441
- Truffer M, Kääb A, Harrison WD, Osipova GB, Nosenko GA, Espizua L, Gilbert A, Fischer L, Huggel C, Craw Burns PA and Lai AW (2021) Chapter 13 - Glacier surges. In W Haeberli and C Whiteman (eds.), *Snow and Ice-Related Hazards, Risks, and Disasters (Second Edition)*, Hazards and Disasters Series, 417–466, Elsevier, ISBN 978-0-12-817129-5 (doi: 10.1016/B978-0-12-817129-5.00003-2)
- Truong C, Oudre L and Vayatis N (2019) Supervised kernel change point detection with partial annotations. In *ICASSP 2019-2019 IEEE International Conference on Acoustics, Speech and Signal Processing (ICASSP)*, 3147–3151, IEEE
- Truong C, Oudre L and Vayatis N (2020) Selective review of offline change point detection methods. *Signal Processing*, **167**, 107299
- Vale AB, Arnold NS, Rees WG and Lea JM (2021) Remote detection of surge-related glacier terminus change across High Mountain Asia. *Remote Sensing*, **13**(7), 1309
- Vijay S, Khan SA, Kusk A, Solgaard AM, Moon T and Bjørk AA (2019) Resolving seasonal ice velocity of 45 Greenlandic glaciers with very high temporal details. *Geophysical Research Letters*, **46**(3), 1485–1495
- Xie Z, Haritashya UK, Asari VK, Young BW, Bishop MP and Kargel JS (2020) Glaciernet: A deep-learning approach for debris-covered glacier mapping. *IEEE Access*, **8**, 83495–83510
- Yde JC and Paasche Ø (2010) Reconstructing Climate Change: Not All Glaciers Suitable. *Eos, Transactions American Geophysical Union*, **91**(21), 189–190 (doi: 10.1029/2010EO210001)
- Zhu Q, Ke CQ and Li H (2021) Monitoring glacier surges in the Kongur Tagh area of the Tibetan Plateau using Sentinel-1 SAR data. *Geomorphology*, **390**, 107869